HHS Public Access

Author manuscript

Nature. Author manuscript; available in PMC 2021 June 16.

Published in final edited form as:

Nature. 2021 January ; 589(7842): 456–461. doi:10.1038/s41586-020-03056-z.

Sorting Nexin 5 Mediates Virus-Induced Autophagy and Immunity

Xiaonan Dong[1], **Yuting Yang**[1], **Zhongju Zou**[1,2], **Yuting Zhao**[1], **Bo Ci**[3], **Lin Zhong**[3], **Madhura Bhave**[4], **Liwei Wang**[5], **Yi-Chun Kuo**[5], **Xiao Zang**[3], **Rui Zhong**[3], **Elizabeth R. Aguilera**[6], **R. Blake Richardson**[6], **Boris Simonetti**[7], **John W. Schoggins**[6], **Julie K. Pfeiffer**[6], **Li Yu**[8], **Xuewu Zhang**[5], **Yang Xie**[3,9], **Sandra L. Schmid**[4], **Guanghua Xiao**[3,9], **Paul A. Gleeson**[10], **Nicholas T. Ktistakis**[11], **Peter J. Cullen**[7], **Ramnik J. Xavier**[12,13,14,*], **Beth Levine**[1,2,6]

[1]Center for Autophagy Research, Department of Internal Medicine, University of Texas Southwestern Medical Center, Dallas, Texas 75390, USA

[2]Howard Hughes Medical Institute, University of Texas Southwestern Medical Center, Dallas, Texas 75390, USA

[3]Quantitative Biomedical Research Center, Department of Population and Data Sciences, University of Texas Southwestern Medical Center, Dallas, Texas 75390, USA

[4]Department of Cell Biology, University of Texas Southwestern Medical Center, Dallas, Texas 75390, USA

[5]Department of Pharmacology, University of Texas Southwestern Medical Center, Dallas, Texas 75390, USA

[6]Department of Microbiology, University of Texas Southwestern Medical Center, Dallas, Texas 75390, USA

[7]School of Biochemistry, University of Bristol, Bristol BS8 1TD, UK

[8]The State Key Laboratory of Membrane Biology, Tsinghua University-Peking University Joint Centre for Life Sciences, School of Life Sciences, Tsinghua University, Beijing 100084, China

[9]Harold C. Simmons Comprehensive Cancer Center, University of Texas Southwestern Medical Center, Dallas, Texas 75390, USA

[10]Department of Biochemistry and Molecular Biology and Bio21 Molecular Science and Biotechnology Institute, The University of Melbourne, Victoria 3010, Australia

[*]Correspondence to: xavier@molbio.mgh.harvard.edu.

Author contributions: X.D. and B.L. designed the study; X.D., Y.K., B.S., J.W.S., J.K.P., L.Y., X.Z., S.L.S., P.A.G., N.T.K., P.J.C., R.J.X. and B.L. developed methodology; Y.Z. purified PI3KC3-C1 and PI3KC3-C2 complexes; L.W. purified SNX5 proteins; M.B. performed transferrin receptor recycling assay and EGFR endolysosomal degradation assay; E.R.A. and R.B.R. performed infection with CVB3, poliovirus, IAV and Zika virus; X.D., Y.Y. and Z.Z., performed animal study, viral growth curves, GFP-LC3 puncta quantitation, co-IP experiments and western blot experiments; X.D. performed siRNA screens and all the other experiments in this study; X.D., B.C., L.Z., X.Z., R.Z., Y.X., and G.X. analyzed the data; X.D. and B.L. wrote the manuscript; R.J.X. contributed to and supervised the manuscript resubmission. Beth Levine passed away in June 2020.

Competing interests: Beth Levine is a scientific co-founder of Casma Therapeutics, Inc. Ramnik J. Xavier is co-founder of Jnana Therapeutics and Celsius Therapeutics. None of these companies provided support for this work.

[11]Signalling Programme, The Babraham Institute, Cambridge CB22 4AT, UK

[12]Center for Computational and Integrative Biology, Massachusetts General Hospital, Harvard School of Medicine, Boston, Massachusetts 02114, USA

[13]Department of Molecular Biology, Massachusetts General Hospital and Harvard Medical School, Boston, Massachusetts 02114, USA

[14]Broad Institute of MIT and Harvard University, Cambridge, Massachusetts 02142, USA

Abstract

Autophagy, a lysosomal degradation pathway, plays an essential role in multiple aspects of immunity, including immune system development, regulation of innate and adaptive immune and inflammatory responses, selective degradation of intracellular microbes, and host protection against infectious diseases[1,2]. Unlike autophagy induction by stimuli such as nutrient deprivation and mTOR suppression, little is known about how autophagosomal biogenesis is initiated in mammalian cells in response to viral infection. We performed genome-wide siRNA screens and found that the endosomal protein sorting nexin 5 (SNX5)[3,4] is essential for virus-induced, but not for basal, stress- or endosome-induced, autophagy. We showed that *SNX5* deletion increases cellular susceptibility to viral infection *in vitro*, and that *Snx5* knockout in mice enhances lethality after infection with multiple human viruses. Mechanistically, SNX5 interacts with beclin 1 and ATG14-containing Class III phosphatidylinositol 3-kinase (PI3KC3) complex 1 (PI3KC3-C1), increases the lipid kinase activity of purified PI3KC3-C1, and is required for endosomal generation of PI3P and recruitment of the PI3P-binding protein WIPI2 to virion-containing endosomes. These findings identify a context- and organelle-specific mechanism – SNX5-dependent PI3KC3-C1 activation at endosomes – for autophagy initiation during viral infection.

To identify cellular factors required for virus-induced autophagy, we performed high-content image-based genome-wide siRNA screens in HeLa cells infected with Sindbis virus (SIN) (an enveloped single-stranded RNA virus) and a genetically engineered strain of herpes simplex virus type 1 (HSV-1) (an enveloped double-stranded DNA virus). The latter contains a deletion in the beclin 1-binding domain (BBD) of the HSV-1 neurovirulence protein ICP34.5 that prevents it from inhibiting host autophagy (HSV-1ΔBBD)[5]. The autophagy pathway targets these viruses *in vitro*, protecting mice against lethal central nervous system (CNS) infection[5–7]. Both viruses induce autophagy in HeLa and HeLa/GFP-LC3 cells as demonstrated by increased GFP-LC3 (a marker of autophagosomes) puncta, increased conversion of LC3-I to the lipidated autophagosome-associated form LC3-II; and degradation of the autophagy substrate p62/SQSTM1 (Extended Data Fig. 1a–i). These changes reflect autophagic flux, as GFP-LC3 puncta and LC3-II accumulation increased further upon lysosomal inhibition with bafilomycin A1, which also decreased p62/SQSTM1 degradation. This autophagic flux was reduced by siRNA knockdown of essential autophagy genes *ATG7* and *ATG13*, as well as pharmacological inhibition with the Class III phosphatidylinositol-3 kinase (PI3KC3, also known as PIK3C3 or VPS34) inhibitor, PIK-III (Extended Data Fig. 1). These results indicate a role for the autophagy protein conjugation systems, the autophagy-initiating ULK1 complex and the PI3KC3 complex, involved in autophagosome membrane nucleation, in virus-induced autophagy.

Primary screens of a pooled siRNA oligonucleotide library targeting 18,115 unique human genes showed that knockdown of 310 genes resulted in fewer GFP-LC3 puncta in SIN- and/or HSV-1ΔBBD-infected HeLa/GFP-LC3 cells but not in mock-infected cells (Extended Data Fig. 2a–e). We performed deconvolution screens with four individual siRNA oligonucleotides per candidate gene. Gene knockdown with two or more siRNA oligonucleotides decreased numbers of virus-induced GFP-LC3 puncta for 216 of 310 (69.7%) genes (confirmed hits) (Fig. 1a, Extended Data Fig. 2f, g).

Bioinformatic analyses showed enrichment for gene sets associated with biological processes and molecular functions, including protein complex assembly, transport, kinases and certain transcription factors (Extended Data Fig. 2h, i), as well as NLRX1 which promotes virus-induced autophagy[8]. We focused on endosomal proteins, as most viruses enter cells through a route that converges at the endolysosomal system[9]. Cytoplasmic entry of SIN and HSV-1ΔBBD via fusion at the plasma membrane resulted in fewer GFP-LC3 puncta than normal entry (Extended Data Fig. 3a–d), underscoring the importance of endosomal entry for virus-induced autophagy. We focused further analyses on the endosomal protein sorting nexin 5 (SNX5). SNX5 encodes a predicted Phox (PX) domain, a conserved protein domain that binds phosphoinositides, such as phosphatidylinositol 3-phosphate (PI3P). Additionally, SNX5 contains a Bin/Amphiphysin/Rvs (BAR) domain, which is essential for sensing and driving membrane curvature[10,11]. Critical early events during autophagosomal biogenesis include PI3P generation by the PI3KC3 complex I (PI3KC3-C1, also known as PIK3C3-C1) and membrane remodeling[12]. Thus, we hypothesized that SNX5 might act during viral endosomal entry to increase endosome-based PI3P generation and initiate autophagosome formation.

Knockdown of *SNX5*, and the related gene *SNX32*, decreased SIN- and HSV-1ΔBBD-induced autophagy by a magnitude similar to *ATG7* knockdown (Fig. 1b, Extended Data Fig. 3e–i). Importantly, siRNA knockdown of *SNX5* or *SNX32* decreased autophagy induction by six additional pathogenic human viruses, including Zika virus[13], West Nile virus (WNV)[14], chikungunya virus (CHIKV)[15], poliovirus[16], Coxsackievirus B3 (CVB3)[17] and influenza A virus (IAV)[18] (Fig. 1b, Extended Data Fig. 3e–i). To rule out off-target siRNA effects, we generated HeLa $SNX5^{KO}$ cells using the CRISPR/Cas9 system and stably transfected them with GFP-LC3 (Extended Data Fig. 3j). $SNX5^{KO}$/GFP-LC3 cells were deficient in SIN- and HSV-1ΔBBD-induced autophagy, but this defect was fully rescued by reconstitution of wild-type SNX5 in two independent $SNX5^{KO}$/GFP-LC3/SNX5 cell clones (Extended Data Fig. 3k). These results indicate that SNX5 is required for autophagy induced by a broad range of viral pathogens.

Neither siRNA knockdown of *SNX5* or *SNX32*, nor CRISPR knockout of *SNX5*, altered basal autophagy, starvation-induced autophagy, or mTOR inhibition-induced autophagy (Extended Data Fig. 4a–c). $SNX5^{KO}$ and wild-type HeLa/GFP-LC3 cells showed identical formation of LC3-positive Group A *Streptococcus* containing vacuoles[19] (Extended Data Fig. 4d, e), indicating that xenophagy of a bacterium that enters cells by endosomes does not require SNX5. SNX5 was also dispensable for osmotic stress-induced LC3-recruitment to endolysosomal structures labeled by EEA1 and LAMP1[20] (Extended Data Fig. 4f, g). Furthermore, $SNX5^{KO}$ and wild-type HeLa cells exhibited similar monensin-induced LC3

recruitment to latex bead-containing phagosomes, an assay for measuring LC3-associated phagocytosis (LAP) in non-phagocytic cells[21] (Extended Data Fig. 4h, i). Thus, SNX5 is specific for virus-induced autophagy, and is not required for general autophagy or non-canonical forms of autophagy that require endolysosomal or phagosomal LC3 recruitment.

siRNA knockdown of the essential retromer gene *VPS29* did not alter virus-induced autophagy (Fig. 1b, Extended Data Fig. 3e, h), but impaired retromer-dependent retrograde transport of glucose transporter 1 (GLUT1) as demonstrated by increased lysosomal localization of mis-sorted GLUT1 (Extended Data Fig. 5a–f). Consistent with the reported functional redundancy of SNX5, SNX6 and SNX32 in retromer activity[4,22], neither knockdown of *SNX5* nor *SNX32* impaired GLUT1 trafficking. Early endocytic function was identical in *SNX5*^{KO} and wild-type HeLa cells, as measured by recycling kinetics of the transferrin receptor (Extended Data Fig. 5g–i). Late endocytic function also remained unchanged in *SNX5*^{KO} cells, as measured by rates of epidermal growth factor receptor (EGFR) degradation (Extended Data Fig. 5j, k). Thus, the requirement for SNX5 in virus-induced autophagy is unlikely related to a role in retromer function or other endocytic functions.

Since autophagy restricts the replication of certain viruses *in vitro* and protects against certain viral diseases *in vivo*[1,2], we studied viral infection in SNX5-deficient cells and pathogenesis in *Snx5*$^{-/-}$ mice[23]. We focused on SIN, HSV-1ΔBBD, WNV, and CHIKV viruses for which existing data indicate the importance of autophagy in controlling viral disease[5–7,15,24,25]. For the first three, which are neuronotropic and cause fatal encephalitis in mice, we used an intracranial model of *in vivo* infection to study virus-host interactions in neurons without confounding effects of other stages of pathogenesis, including viral dissemination from the periphery and systemic immune responses that do not penetrate the blood-brain barrier. For CHIKV, we used an established model of peripheral viral infection in neonatal mice, as previous studies have reported a protective role of autophagy[15,25]. *SNX5* deletion in HeLa cells increased susceptibility to SIN, HSV-1ΔBBD, WNV and CHIKV infection in viral infectivity assay (Extended Data Fig. 6a–d). Viral multi-step growth also increased in *SNX5*^{KO} cells (Extended Data Fig. 6e–h), as well as in primary mouse embryonic fibroblasts (MEFs) derived from *Snx5*$^{-/-}$ compared to wild-type littermates (Extended Data Fig. 6i–l). Viral infectivity and replication was not increased in *SNX5*^{KO} cells or *Snx5*$^{-/-}$ MEFs after infection with autophagy-suppressing viruses, including SIN.dnAtg5 (expressing a dominant negative Atg5) and HSV-1ΔBBD-MR (a marker-rescued strain of HSV-1ΔBBD expressing wild-type ICP34.5, which inhibits host autophagy by binding beclin 1) (Extended Data Fig. 6m–r). Increased viral replication in SNX5 deficiency was not due to alterations in viral entry (Extended Data Fig. 6s, t) or virus-induced interferon signaling (Extended Data Fig. 6u, v), and *SNX5* mRNA did not decrease upon infection (Extended Data Fig. 6w). Therefore, SNX5 restricts viral replication in a cell autonomous fashion by an autophagy-dependent mechanism.

Neonatal *Snx5*$^{-/-}$ mice were more susceptible to lethal infection with SIN, CHIKV, or WNV than *Snx5*$^{+/+}$ counterparts, and adult *Snx5*$^{-/-}$ mice were more susceptible to lethal HSV-1ΔBBD encephalitis than their wild-type littermates (Fig. 1c). The brains of neonatal SIN-infected and adult HSV-1ΔBBD-infected *Snx5*$^{-/-}$ mice revealed increased viral titers

and neuronal death at certain time points after infection (Extended Data Fig. 7a–f). This *Snx5*-mediated protective effect is likely related to autophagy induction, as mortality did not differ between *Snx5*$^{+/+}$ and *Snx5*$^{-/-}$ mice infected with SIN.dnAtg5 or HSV-1ΔBBD-MR that inhibit neuronal autophagy[5,6] (Fig. 1c, Extended Data Fig. 7g). Thus, *Snx5* is a previously undescribed host factor that functions in antiviral defense *in vivo.*

We evaluated whether SNX5 interacts with autophagy-specific PI3KC3-C1 complexes, which function in autophagosome initiation or PI3KC3-C2 complexes, which function in autophagosome maturation and endocytic trafficking[12]. As demonstrated by the presence of ATG14, but not UVRAG (Fig. 2a), only PI3KC3-C1 complexes co-immunoprecipitated with SNX5. This difference is not due to alterations in assembled PI3KC3-C1 or PI3KC3-C2 complexes, as both ATG14 and UVRAG co-immunoprecipitated with beclin 1 (Fig. 2b). The SNX5-PI3KC3-C1 interaction does not require PI3KC3-C1 lipid kinase activity, as it is not diminished by treatment with the PI3KC3-specific inhibitor PIK-III (Fig. 2a, b), which blocks autophagy during baseline conditions, starvation, mTOR inhibition, and viral infection (Extended Data Figs. 1l, 8a–e). Recombinant SNX5 interacts with intact PI3KC3-C1, but not PI3KC3-C2, complexes (Fig. 2c–e, Extended Data Fig. 8f), indicating a direct SNX5-PI3KC3-C1 interaction. The interaction specificity may represent binding of SNX5 to the PI3KC3-C1-specific protein ATG14, an autophagy protein that senses membrane curvature[26], or other conformational differences between PI3KC3-C1 and PI3KC3-C2[27,28].

Our findings suggest that SNX5 acts upstream of PI3P generation to regulate PI3KC3-C1 activation during viral infection. We therefore studied the effects of recombinant SNX5 on the lipid kinase activity of Large Unilamellar Vesicles prepared by Extrusion Technique (LUVETs)[29,30] with two distinct membrane curvatures employing a lipid mixture that resembles endosomal lipid composition[31,32]. On smaller LUVETs, PI3KC3-C1 complexes exhibited approximately three-fold higher lipid kinase activity which was abolished by PIK-III (Fig. 2f). Compared to SUMO control protein (Fig. 2c), recombinant SUMO-SNX5 increased PI3KC3-C1 activity on larger LUVETs in a dose-dependent manner (Fig. 2g, left); the magnitude of this effect was decreased on smaller LUVETs with greater membrane curvature (Fig. 2g, right).

Positively charged residues in the concave surface of BAR domains mediate membrane association of BAR-containing proteins via electrostatic interaction with the lipid bilayer[11]. K429E, K430E and R431E mutations in the BAR domain of SNX1, a sorting nexin closely related to SNX5, block its association with membranes and the ability to induce membrane remodeling[33]. To investigate whether the corresponding positively charged BAR domain residues in SNX5 are required for its effect on PI3KC3-C1 activity, we aligned amino acid sequences of SNX5 and SNX1 and identified residues K328, R330 and K332, which were substituted with glutamic acid (SNX5 EEE) (Extended Data Fig. 8g, h). Unlike wild-type SUMO-SNX5, the EEE mutant protein failed to enhance PI3KC3-C1 activity on larger LUVETs (Fig. 2g). SUMO-SNX5 EEE did not bind PI3KC3-C1 complexes (Fig. 2e), indicating that the tip region of the BAR domain carrying these evolutionarily conserved residues is required for interaction with PI3KC3-C1. A previous study revealed that PI3KC3-C1 has diminished capacity to generate PI3P on low-curvature membranes such as giant unilamellar vesicles[28]. Our data suggest that SNX5, by enhancing local membrane

curvature through its BAR domain, facilitates PI3KC3-C1-mediated PI3P generation on flatter membranes that resemble the endosome.

We next performed cryogenic electron microscopy (cryo-EM) of the larger LUVETs incubated with SUMO-SNX5, SUMO-SNX5 EEE or SUMO control protein. In the presence of SNX5, but not SUMO-SNX5 EEE, liposomes had increased membrane curvature (Fig. 2h, i). Thus, at least *in vitro*, the SNX5 BAR domain is required for increasing liposomal membrane curvature, a mechanism essential for increased PI3KC3-C1 activity.

Virally-infected *SNX5*^{KO} cells were defective in endosomal PI3P production, as measured both by staining with a fluorescent PI3P-binding probe, PX-Alexa555[28], and immunostaining for WIPI2, a PI3P-binding protein and early autophagosome marker[34]. Defects occurred during SIN and HSV-1ΔBBD infection, but not at baseline, or upon induction of autophagy by starvation or mTOR inhibition. The PI3P production defect was rescued by wild-type SNX5 but not mutant SNX5 EEE (Extended Data Fig. 9). SIN and HSV-1ΔBBD infection increased WIPI2 puncta that colocalized with EEA1 in parental wild-type and *SNX5*^{KO} cells reconstituted with wild-type SNX5, but not in *SNX5*^{KO} cells or *SNX5*^{KO} cells reconstituted with SNX5 EEE (Fig. 3a, b). The defect in endosomal WIPI2 puncta formation in *SNX5*^{KO} cells was not related to decreased endosomal localization of beclin 1, ATG14 or VPS34 (Extended Data Fig. 10a). Similar to GFP-LC3 puncta (Extended Data Fig. 1l), the SIN- and HSV-1ΔBBD-induced increase of the PI3P probe signal and WIPI2 puncta formation in HeLa cells was abolished by PIK-III (Extended Data Fig. 10b–e). Thus, SNX5 – and residues in its BAR domain predicted to sense and drive membrane curvature – are not required for the endosomal localization of PI3KC3-C1, but are required for the endosomal function of PI3KC3-C1 and PI3P generation in virally-infected cells.

To determine the location of SNX5-dependent PI3KC3-C1 activation, we employed a Sindbis virus strain expressing mCherry fused to the E2 envelope glycoprotein (SIN.mCherry-E2)[35]. One hour after infection, SIN.mCherry-E2 was present in EEA1-positive endosomes, representing endocytosed virions (Fig. 3c). An increased percentage of mCherry-E2-positive EEA1-positive structures with colocalized SNX5 puncta relative to mCherry-E2-negative EEA1-positive structures (Fig. 3c–e) indicates selective recruitment of SNX5 to virion-containing endosomes. Similarly, more colocalized WIPI2 puncta (Fig. 3f, g) indicates the selective generation of PI3P at virion-containing endosomes. WIPI2 puncta formation at virion-containing endosomes decreased in SIN.mCherry-E2-infected *SNX5*^{KO} cells; this defect was rescued by wild-type SNX5 but not SNX5 EEE (Fig. 3f, g). Thus, SNX5 functions specifically at virion-containing endosomes to increase PI3KC3-C1 activity and autophagosomal biogenesis.

Our findings suggest that stimuli inside an organelle may be linked to organelle-specific initiation of autophagosomal biogenesis. When viruses enter endosomes, SNX5, a protein that senses and drives membrane curvature, specifically localizes to virion-containing early endosomes and functions to initiate activation of the ATG14-containing PI3KC3-C1 complex, the first stage of autophagosome formation. This mechanism is unique to viral infections and not to other forms of stress-induced autophagy (e.g. nutrient deprivation and mTOR inhibition) or non-canonical forms of autophagy (e.g. bacterial xenophagy, osmotic

stress-induced autophagy and LAP), suggesting distinct cellular mechanisms for activating PI3KC3-C1 and autophagy in response to different stress stimuli. We speculate that as-of-yet unidentified proteins that regulate membrane curvature (or other factors that locally govern PI3KC3-C1 activity) serve as crucial mediators of stimulus-specific autophagy.

The question of how luminal viruses stimulate the SNX5-PI3KC3 axis on the cytoplasmic face of endosomes remains outstanding. Based on insights from other experimental systems[22], SNX5 may associate with an array of integral membrane proteins to establish a "signature" for virion-containing endosomes. Evidence that the human cytomegalovirus tegument protein UL35 antagonizes SNX5-mediated antiviral activity[36] and that SIN replication is attenuated in *SNX5*^{KO} HEK293T cells[37] suggests evolutionarily conserved complex mechanisms by which SNX5 mediates host-virus interactions. Additional structural and microscopy-based studies, requiring development of specific immuno-electron microscopy-based tools, will be needed to capture the transient interaction of SNX5 with virion-containing endosomal membranes and to dissect the precise molecular mechanisms underlying this process.

Methods

Mammalian cell lines and cell culture

All cell culture reagents including media, sera, antibiotics and trypsin-EDTA (0.25%), were purchased from Invitrogen/Gibco (Thermo Fisher Scientific) unless otherwise specified. Primary mouse embryonic fibroblasts (MEFs) were isolated from *Snx5*$^{+/+}$ and *Snx5*$^{-/-}$ littermate offspring on embryonic day (E) 13.5 as previously described[39]. HeLa, BHK-21, Vero and 293T cell lines were obtained from American Type Culture Collection (ATCC), which have been thoroughly tested and authenticated by ATCC. Additional authentication of HeLa cells was performed by the ATCC Cell Line Authentication Service using short-tandem repeat profiling (STR) analysis. Vero E6 cell line was a gift from Matthew B. Frieman (University of Maryland), which originally sourced from ATCC (CRL-1586) and was not further authenticated. MDCK cell line was a gift from Charles M. Rice (The Rockefeller University), which was authenticated as canine origin by cloning and sequencing immune genes from stimulated cells. HEK293F cell line was a gift from Hongwei Wang (Tsinghua University). All the cell lines used in this study tested negative for mycoplasma contamination using PCR-based Venor GeM Mycoplasma Detection Kit (Sigma-Aldrich MP0025). All the cell lines were cultured and maintained according to ATCC's instructions, and used at low passage numbers. HeLa cell clones were cultured in Opti-MEM I Reduced Serum Medium supplemented with 5% fetal bovine serum (FBS), 100 units/mL penicillin and 100 μg/mL streptomycin. MEFs, BHK-21 cells, Vero cells, Vero E6 cells, MDCK cells and HEK293T cells were cultured in Dulbecco's Modified Eagle Medium (DMEM) supplemented with 10% FBS, 100 units/mL penicillin and 100 μg/mL streptomycin. Media supplemented with heat-inactivated (HI) FBS were used for viral infection experiments. HEK293F cells were cultured in SMM293-TI medium (Sino Biological) supplemented with 100 units/mL penicillin and 100 μg/mL streptomycin. HeLa/GFP-LC3 cells that stably express GFP-LC3 were generated by transfecting HeLa cells with a plasmid pIRES.GFP-LC3.neo3 and selection in medium containing 500 ng/mL geneticin.

HeLa *SNX5* CRISPR knockout cell lines (HeLa $SNX5^{KO}$) were generated by CRISPR/Cas9-induced double-strand break at the Genome Engineering and iPSC Center (GEiC) of Washington University School of Medicine (St. Louis, MO). Sequences encompassing candidate guide RNA (gRNA) sites were analyzed for common (>1%) single nucleotide polymorphisms (SNPs) using the UCSC Genome Browser (https://genome.ucsc.edu), and no common SNPs were detected in the selected two gRNAs for the target gene. The sequences of gRNAs used for CRISPR knockout are as follows: *SNX5* exon5.g7: 5'-CCGCTGAAGAAAGACTTCATNGG-3' and *SNX5* exon5.g8: 5'-CTGAAGAAAGACTTCATGGGNGG-3'. Frequencies of local insertions and deletions (indels) in a *SNX5* CRISPR knockout clone were determined using targeted deep sequencing, which confirmed the gRNA-targeted *SNX5* deletion in the HeLa cell genome. Reconstituted HeLa $SNX5^{KO}$/SNX5 cells, HeLa $SNX5^{KO}$/SNX5 EEE cells, HeLa $SNX5^{KO}$/vector cells, and HeLa WT/vector control cells were generated by infection with retroviruses expressing wild-type human SNX5, SNX5 EEE mutant (K328E/R330E/K332E; Extended Data Fig. 8g, h), or an empty vector, which was followed by selection in medium containing 500 ng/mL puromycin. HeLa $SNX5^{KO}$/GFP-LC3 cells were generated by transfecting HeLa $SNX5^{KO}$ cells with a plasmid pIRES.GFP-LC3.neo3 and selection in medium containing 500 ng/mL geneticin. Reconstituted HeLa $SNX5^{KO}$/GFP-LC3/SNX5 cells were generated by transfecting HeLa $SNX5^{KO}$/GFP-LC3 cells with a plasmid pIRES.SNX5.puro3 and selection in medium containing 500 ng/mL puromycin. For viral infection experiments using the stable cell lines described above, selection antibiotics (such as geneticin or puromycin) were withdrawn from the culture media for at least 24 h prior to viral infection.

Mouse strains

C57BL/6J mice were obtained from The Jackson Laboratory and all mouse strains used in this study were backcrossed to female C57BL/6J breeders for more than ten generations. $Snx5^{-/-}$ mice were generated by the UC DAVIS Knockout Mouse Project (KOMP) Repository (https://www.komp.org/) and have been previously described[23]. Genomic DNA from mice was prepared from mouse tail using DirectPCR Lysis Reagent (Viagen Biotech) and Proteinase K (Roche). Mouse genotypes were determined by PCR using TaKaRa SapphireAmp Fast PCR Master Mix (Clontech) and the following primer pairs: *Snx5* WT-1, 5'-GCTTTGCCTCTGATTTGGATCTCC-3'; *Snx5* WT-2, 5'-CTAAGACAATAAAACCCACCGGGCG-3'; *Snx5* KO-1, 5'-GACATGAGCACACTGTTAGTGCAGG-3'; *Snx5* KO-2, 5'-GAGATGGCGCAACGCAATTAATG-3'. The PCR conditions are as follows: 1 min at 94°C, 35 cycles of amplification stage (5 sec at 98°C, 5 sec at 55°C and 5 sec at 72°C) and 5 min at 72°C. $Snx5^{+/+}$ genomic DNA yields a 405-bp band; $Snx5^{-/-}$ genomic DNA yields a 386-bp band; $Snx5^{+/-}$ genomic DNA yields both a 405-bp band and a 386-bp band.

Chemicals

Bafilomycin A1 (Baf A1; Sigma-Aldrich B1793), a lysosomal inhibitor, was dissolved in sterile-filtered DMSO (Sigma-Aldrich D2650) as a 100 μM stock solution. Cycloheximide (Sigma-Aldrich C7698) was dissolved in sterile water as a 10 mg/mL stock solution and then passed through a 0.22-μm filter. Monensin (Sigma-Aldrich M5273) was dissolved in ethanol (Thermo Fisher Scientific) as a 50 mg/mL (72.2 mM) stock solution. PIK-III

(Selleck Chemicals S7683), a PI3KC3 (VPS34)-specific inhibitor[40], was dissolved in sterile-filtered DMSO as a 4 mM stock solution. Torin 1 (Selleck Chemicals S2827), an mTOR inhibitor[41], was dissolved in sterile-filtered DMSO as a 1 mM stock solution. All stock solutions were stored in small aliquots at −20°C. For control groups of chemical treatment, equivalent volume of according chemical-free sterile solvent was added into culture media.

Antibodies

The following commercial antibodies (vendor, catalog number and dilution) were used for immunoprecipitation, western blot analyses and immunofluorescence staining according to manufacturers' instructions: mouse anti-actin monoclonal antibody (Sigma-Aldrich A1978, 1:1000), mouse anti-actin monoclonal antibody (C4) HRP (Santa Cruz Biotechnology sc-47778 HRP, 1:5000), rabbit anti-ATG7 polyclonal antibody (Sigma-Aldrich A2856, 1:1000), rabbit anti-ATG13 monoclonal antibody (Abcam ab201467, 1:2000), mouse anti-ATG14 monoclonal antibody (MBL International Corporation M184-3, 1:500 for western blot and 1:1000 for immunofluorescence staining), rabbit anti-ATG14 polyclonal antibody (Cell Signaling Technology 5504S, 1:500), mouse anti-beclin 1 monoclonal antibody (E-8) (Santa Cruz Biotechnology sc-48341, 1:1000 for western blot and 1:100 for immunoprecipitation), rabbit anti-beclin 1 polyclonal antibody (H-300) (Santa Cruz Biotechnology sc-11427, 1:1000), goat anti-EEA1 polyclonal antibody (N-19) (Santa Cruz Biotechnology sc-6415, 1:200), rabbit anti-EEA1 polyclonal antibody (H-300) (Santa Cruz Biotechnology sc-33585, 1:200), rabbit anti-EGFR monoclonal antibody (Cell Signaling Technology 4267S, 1:1000), rabbit anti-GLUT1 polyclonal antibody (Abcam ab15309, 1:500), mouse 6×-His tag monoclonal antibody (HIS.H8) (Thermo Fisher Scientific MA1-21315, 1:500), goat anti-LAMP1 polyclonal antibody (C-20) (Santa Cruz Biotechnology sc-8098, 1:200), rabbit anti-LC3B polyclonal antibody (Novus Biologicals NB100-2220, 1:2000), guinea pig anti-p62/SQSTM1 (C-terminus) polyclonal serum (Progen GP62-C, 1:1000), mouse anti-p62/SQSTM1 monoclonal antibody (Abnova H00008878-M01, 1:5000), goat anti-SNX5 polyclonal antibody (Abcam ab5983, 1:100 for both immunoprecipitation and western blot), mouse anti-SNX5 monoclonal antibody (F-11) (Santa Cruz Biotechnology sc-515215, 1:400 for western blot and 1:200 for immunofluorescence staining), rabbit anti-UVRAG monoclonal antibody (D2Q1Z) (Cell Signaling Technology 13115, 1:500), rabbit anti-UVRAG polyclonal antibody (Sigma-Aldrich U7508, 1:1000), rabbit anti-VPS29 polyclonal antibody (Abcam ab98929, 1:500), rabbit anti-VPS34 monoclonal antibody (D9A5) (Cell Signaling Technology 4263S, 1:100 for western blot and 1:200 for immunofluorescence staining), mouse anti-WIPI2 monoclonal antibody (Bio-Rad Laboratories MCA5780GA, 1:200), normal goat IgG (Abcam ab37373, 1:1000), normal mouse IgG (Santa Cruz Biotechnology sc-2025, 1:200), donkey anti-goat IgG-HRP (Santa Cruz Biotechnology sc-2056, 1:1000), goat anti-guinea pig IgG H&L (HRP) (Abcam ab6908, 1:2000), peroxidase AffiniPure goat anti-mouse IgG Fcγ fragment specific antibody (Jackson ImmunoResearch Laboratories 115-035-071, 1:2000), donkey anti-rabbit IgG HRP-conjugate species-adsorbed (EMD Millipore AP182P, 1:2000), donkey anti-goat IgG (H+L) cross-adsorbed secondary antibody Alexa Fluor 594 (Thermo Fisher Scientific A11058, 1:1000), donkey anti-goat IgG (H+L) cross-adsorbed secondary antibody Alexa Fluor 647 (Thermo Fisher Scientific A-21447, 1:1000), donkey anti-mouse IgG (H+L) highly cross-adsorbed secondary antibody Alexa Fluor 488 (Thermo Fisher Scientific

A21202, 1:1000), donkey anti-rabbit IgG (H+L) highly cross-adsorbed secondary antibody Alexa Fluor 488 (Thermo Fisher Scientific A-21206, 1:1000), and donkey anti-rabbit IgG (H +L) highly cross-adsorbed secondary antibody Alexa Fluor 594 (Thermo Fisher Scientific A21207, 1:1000).

Bacteria

Streptococcus pyogenes (also known as Group A *Streptococcus*) wild-type serotype M6 strain JRS4 ($M6^+F1^+$) and the isogenic mutant JRS4ΔSLO were kindly provided by Ichiro Nakagawa (Kyoto University)[19]. JRS4ΔSLO lacks the gene streptolysin O (*SLO*), a cholesterol-dependent pore-forming exotoxin, and thus does not escape from endosomes and induce Group A *Streptococcus*-containing autophagosome-like vacuoles (GcAVs) in HeLa cells[19]. Group A *Streptococcus* strains were amplified in BBL Brain Heart Infusion medium (Becton, Dickinson and Company) in a 5% CO_2 incubator. For subcloning, Invitrogen MAX Efficiency DH5α Competent Cells (Thermo Fisher Scientific) were transformed with plasmids and selected on LB agar plates with certain selection antibiotics. Isolated single colonies were cultured in Difco Terrific Broth medium (Becton, Dickinson and Company) in an Innova 43 Incubator Shaker (New Brunswick Scientific). Bacterial plasmids for cloning experiments were amplified using a Plasmid Midi Kit (QIAGEN) and stored in −20°C. The insertion fragment in a plasmid was confirmed by Sanger sequencing.

Viral strains

A herpes simplex virus type 1 (HSV-1) mutant strain (HSV-1ΔBBD) was previously genetically engineered to expresses a neurovirulent factor ICP34.5 mutant that lacks the beclin 1-binding domain (BBD) and is unable to suppress autophagy[5,42]. A marker-rescued HSV-1 control strain (HSV-1ΔBBD-MR) expressing wild-type ICP34.5 was generated in parallel and shown to suppress autophagy in both cultured neuronal cells and brains of intracerebrally infected mice[5]. The Sindbis virus (SIN) strain SVIA (ATCC) was derived from a low-passage isolate of the wild-type SIN strain AR339[43]. In this study, the SIN strain used in the majority of cell culture infection experiments was SVIA unless otherwise specified. The recombinant SIN strain with a double subgenomic promoter generated from the SIN vector, dsTE12Q, was previously described[44], as was the recombinant SIN strain dsTE12Q.dnAtg5 (SIN.dnAtg5), which expresses a dominant negative mutant of autophagy core machinery protein, Atg5 K130R, from the second subgenomic promoter, and has been previously shown to inhibit autophagy in brains of intracerebrally infected mice[6]. Recombinant SIN strains, SIN.dnAtg5 and its parental wild-type control dsTE12Q, were used in animal experiments (Fig. 1c, Extended Data Fig. 7a–c) and some *in vitro* experiments (Extended Data Fig. 6m, o, q). The recombinant SIN strain SIN.mCherry-E2 that express mCherry-fused envelope glycoprotein E2 was previously described[35]. The following additional viral strains were used in this study: chikungunya virus (CHIKV) strain 06-021[45] (a gift from Deborah J. Lenschow, Washington University); Coxsackievirus B3 strain H3 (CVB3-H3) generated from an infectious clone (a gift from Marco Vignuzzi, Pasteur Institute); influenza A virus (IAV) strain A/WSN/33 (a gift from Adolfo Garcia-Sastre, Icahn School of Medicine at Mount Sinai); poliovirus generated from the Mahoney type 1 infectious clone (a gift from Karla Kirkegaard, Stanford University); West Nile virus (WNV) strain TX02[46] (a gift from Michael Gale Jr., University of Washington) for infection

of HeLa cells and MEFs; WNV strain Egypt-101[47] (a gift from Michael S. Diamond, Washington University) for mouse infection; and Zika virus strain MR-766 (obtained from Centers for Disease Control and Prevention [CDC]). Viral stocks were propagated and titrated by plaque assays in Vero cells (for HSV-1 and CHIKV), BHK-21 cells (for SIN and WNV), Vero E6 cells (for Zika virus), HeLa cells (for poliovirus and CVB3) and MDCK cells (for IAV), respectively.

Retroviruses for reconstitution of HeLa SNX5^{KO} cell lines

To generate reconstituted HeLa *SNX5*^{KO} cell lines, retroviruses were constructed by co-transfection of HEK293T cells with pCMV-VSV-G (Addgene plasmid #8454), pUMVC (Addgene plasmid #8449), and pBABE-puro empty vector (Addgene plasmid #1764), pBABE-puro-Flag-SNX5 or pBABE-puro-Flag-SNX5 EEE (that carries K328E/R330E/K332E triple mutations) at a mass ratio of 1:9:10 according to Addgene's instructions. Cell culture supernatants were collected at 48 h and 72 h post transfection. Combined supernatants were pre-cleared by centrifugation at 1,000 g and 4°C for 15 min and then passed through sterilized 0.45-μm filters (EMD Millipore). Target cells were infected with fresh media containing retroviral supernatants and 8 μg/mL polybrene (Santa Cruz Biotechnology sc-134220) for 5 h. Retrovirus-containing media were then replaced with fresh virus-free medium, cultured for an additional 48 h, and cells were selected in medium containing 500 ng/mL puromycin.

Small interfering RNAs (siRNAs)

All siRNA oligonucleotides used in this study were synthesized by Dharmacon. The high-content siRNA screens used a genome-wide human siRNA library (siGENOME of Dharmacon) containing 18,115 SMARTpools, in which each pool contains four siRNA oligonucleotides targeting an individual gene. The sequences or catalog number of non-targeting control siRNAs (NC) and gene-specific siRNA oligonucleotides are as follows: NC, 5'-AUCCGCGCGAUAGUACGUA-3' and 5'-UUACGCGUAGCGUAAUACG-3'; *ATG7*, 5'-GGGUUAUUACUACAAUGGUG-3'; *ATG13*, 5'-AGACCAUCUUUGUCCGAAA-3' and 5'-GAAGAAUGUCCGCGAGUUU-3'; *SNX5*, siGENOME siRNA D-012524-01, D-012524-02, D-012524-03 and D-012524-04; *SNX32*, ON-TARGETplus SMARTpool L-017082-01; *VPS29*, ON-TARGETplus SMARTpool L-009764-01.

High-content image-based genome-wide siRNA screens

Primary screens: The siGENOME library siRNA pools were seeded in parallel into nine identical SensoPlate glass-bottom 96-well microplates (Greiner Bio-One 655892) in 25 μL Opti-MEM I Reduced Serum Medium at a final concentration of 50 nM using a BioMek FX Robotic Liquid Handling System (Beckman Coulter Life Sciences), followed by addition of Invitrogen Lipofectamine RNAiMAX (Thermo Fisher Scientific) in 25 μL Opti-MEM I Reduced Serum Medium at a final dilution of 1:500 with an EL406 Washer Dispenser (BioTek Instruments). siRNA oligonucleotides were incubated with Lipofectamine RNAiMAX for 30 min at room temperature, followed by addition of 6,000 HeLa/GFP-LC3 cells in 100 μL Opti-MEM I Reduced Serum Medium supplemented with 5% HI FBS, 100

units/mL penicillin and 100 μg/mL streptomycin (normal medium) using a Multidrop 96/384 Microplate Dispenser (MTX Lab Systems) for reverse transfection. For all the 96-well plates, the first column and the twelfth column were used for on-plate negative and positive controls, which contained alternating wells of non-targeting control siRNAs (NC) and siRNA targeting the essential autophagy gene *ATG7*; and column 2 to column 11 contained siGENOME library siRNA pools (one well/plate/pool). Three sets of triplicate plates (Plate 1 to Plate 3, Plate 4 to Plate 6, and Plate 7 to Plate 9) were used for mock infection, SIN infection and HSV-1ΔBBD infection, respectively. After 48-hour siRNA knockdown, Plate 1 to Plate 3 were mock-infected by dispensing 40 μL/well of virus-free normal medium using an EL406 Washer Dispenser. For the two sets of triplicate plates used for viral infection, the first columns of Plate 4 to Plate 9 were mock-infected by dispensing 40 μL/well of virus-free normal medium (on-plate mock infection controls), and column 2 to column 12 of these plates were infected by dispensing 40 μL/well of normal media containing SIN strain SVIA (at a multiplicity of infection [MOI] of 10) or HSV-1ΔBBD (MOI = 5), respectively. After 1.5-hour incubation at 37°C (viral adsorption and entry), the culture media in all nine plates were replaced with 200 μL/well of fresh normal medium using an EL406 Washer Dispenser. After an additional 2.5-hour incubation at 37°C, 25 μL normal medium containing Invitrogen Hoechst 33342 (Thermo Fisher Scientific) was added to each well (at a final concentration of 5 μg/mL) to stain cellular nuclei. After 20-min additional incubation at 37°C (approximately 4.5 hours post infection [hpi]), medium was aspirated using an EL406 Washer Dispenser and all plates were immediately fixed with 100 μL pre-warmed 3% paraformaldehyde (PFA) (Electron Microscopy Sciences) in 1× Gibco PBS containing Ca^{2+} and Mg^{2+} (Thermo Fisher Scientific) for 20 min at room temperature. The fixation solution was replaced with 1× Gibco PBS (Thermo Fisher Scientific), and all plates were sealed with Microplate Aluminum Tapes (Corning) and stored at 4°C until imaging. All assay plates were imaged within three days after fixation.

High-content automated imaging: Digital images were acquired with a BD Pathway 855 Bioimaging System (BD Biosciences) using an Olympus UAPO/340 40× 340nm air objective (0.9 NA). The microscope filters used for imaging were: Hoechst channel (Ex: 360/10, Dichroic: 400DCLP, Em: 435LP), GFP channel (Ex: 488/10, Dichroic: Fura/FITC, Em: 515LP) and wide-field epifluorescence. Raw micrographs of the Hoechst channel were utilized to determine cell boundaries by a watershed segmentation method, which uses Hoechst-positive nuclei as markers and cytosolic Hoechst signal as the background. After cell segmentation, raw micrographs of the GFP channel were further analyzed to obtain numbers of subcellular GFP-LC3 puncta per cell for each micrograph using the Imaging and Advanced Imaging packages in the software Pipeline Pilot 8.5 (Accelrys). Approximately 250 to 450 cells were analyzed per well.

Assessment of viral infection: To determine whether siRNA knockdown indirectly affected autophagy levels through inhibition of early stages of viral infection (e.g. attachment and uptake), 316 candidate hits from the primary screens were further examined using the same conditions as for the primary screens. Four cherry-picked siRNA library plates (96-well) were generated using the 316 siRNA pools that scored positive in the primary screens. The assay plates were prepared similarly as for the primary screens. Instead

of PFA fixation at 4.5 hpi, assay plates were immediately frozen after incubation with viral inoculum for 1.5 h (1.5 hpi) and stored at −80°C for quantitation of viral loads by plaque assay titration (after three freeze-thaw cycles).

Deconvolution screens: To rule out false-positive hits due to off-target effects of individual siRNA oligonucleotides, 310 candidate genes that passed primary screens were further re-screened for their efficacy in decreasing the number of GFP-LC3 puncta in HeLa/GFP-LC3 cells infected with SIN and HSV-1ΔBBD. Sixteen customized Dharmacon siRNA library plates (96-well) were generated with four siRNA oligonucleotides for each gene (one siRNA oligonucleotide per well). A total of forty wells of NC oligonucleotide was added in the middle of the plates (columns 2 to 11) which served as on-plate negative controls. The assay plates were prepared similarly as for the primary screens, except that individual siRNA oligonucleotides (instead of siRNA pools) were used for gene knockdown.

Quality control (QC) of high-content siRNA screens: Given that 2,268 assay plates (in 35 batches) were used throughout the primary and deconvolution screens, one sentinel assay plate was included for each batch of experiment to monitor batch-to-batch variation. For these sentinel assay plates, NC and siRNAs targeting *ATG7* (48 wells each) were seeded in an alternating pattern on 96-well microplates. All sentinel assay plates were handled together with the set of assay plates for mock infection using the same procedure. After image acquisition and quantitation of numbers of GFP-LC3 puncta, the sensitivity and the specificity of the analysis method was evaluated based on the true positive (*ATG7* siRNA) and true negative (negative control siRNA) wells. The receiver operating characteristic (ROC) curves were plotted (e.g. Extended Data Fig. 2e), and the areas under the curves (AUC) values were calculated to evaluate the screening performance. The ROC mean ± s.d. of all the QC plates was 0.97 ± 0.03, which indicates accuracy and specificity in the identification of cellular factors that regulate numbers of GFP-LC3 puncta.

Statistical analyses of siRNA screens: In the primary siRNA screens, we applied three filters: (1) absence of cytotoxicity of siRNA pools in transfected cells; (2) lack of effect of siRNA pools on numbers of GFP-LC3 puncta in mock-infected cells (basal autophagy); and (3) significant reduction of numbers of GFP-LC3 puncta in cells infected with either SIN or HSV-1ΔBBD (virus-induced autophagy). siRNA pools that have at least two out of three replicate wells with cell numbers less than 100 per montage were considered to have cytotoxic effects in transfected cells and excluded from statistical analyses. To identify siRNA pools that alter only virus-induced autophagy but not basal autophagy, we then performed the following two analyses:

The first analysis used a mixed-effects Poisson regression, where the number of GFP-LC3 puncta in each cell serves as the response variable and the siRNA treatment (using negative control wells as references) serves as the independent variable. A random intercept was included to model the correlated observations among cells within each well. This analysis was performed independently for each of the three screens (mock infection, SIN infection and HSV-1ΔBBD infection) and for each of the triplicate plates of each screen. The coefficient value indicates the magnitude of the effect of an siRNA treatment on numbers of GFP-LC3 puncta compared to that of NC treatment, and the two-sided *P*-value from Wald-

test indicates the statistical significance of the effect. The siRNA pools with either coefficient values greater than log(1/2) (i.e. 50% reduction) or *P*-values greater than 0.05 in at least two out of the three replicate mock infection assay plates were considered as siRNA pools that do not suppress basal autophagy. The siRNA pools with coefficient values less than log(1/2) and *P*-values less than 0.05 in at least two out of the three replicate viral infection assay plates were considered as siRNA pools that suppress SIN-induced autophagy and/or HSV-1ΔBBD-induced autophagy. The siRNA pools that specifically suppress virus-induced autophagy without suppressing basal autophagy were considered as candidate hits in this analysis.

The second analysis also used a mixed-effects Poisson regression, where the number of GFP-LC3 puncta in each cell serves as the response variable. Unlike the first analysis that inspects each plate separately, this analysis used a single integrated model to analyze all nine assay plates from three screens (mock infection, SIN infection and HSV-1ΔBBD infection). Random intercepts were used to take into account correlated observations among cells in the same well or cells in different wells but in the same assay plate. In addition to the main effects of siRNA treatment and viral infections, the fixed effects also included their interactions, the coefficient values of which indicate the difference in the siRNA's effect during viral infections compared to that during mock infection, and the two-sided *P*-values of the interaction terms from Wald-test indicate the statistical significance of such difference. The siRNA pools with coefficient values of the interaction term less than log(1/2) and *P*-values less than 0.05 were considered as candidate hits in this analysis, whose effects on virus-induced autophagy are more pronounced than on basal autophagy.

Both the first analysis and the second analysis described above were performed in open-source R software (www.r-project.org) version 3.1.0 with package lme4 version 1.0-4. The overlapping siRNA pools identified by both statistical analyses were considered as candidate unique hits involved specifically in virus-induced autophagy. The first analysis ensured that scored candidate siRNA pools significantly suppressed virus-induced autophagy at the desired threshold magnitude while not suppressing basal autophagy. The second analysis further ensured that scored candidate siRNA pools led to statistically significantly greater reduction of autophagy (i.e. GFP-LC3 puncta number) during viral infection than during mock infection.

For assessing early stages of viral infection, the relative fold of viral load for each well of the 316 overlapping siRNA pools (that were identified as candidate hits by both statistical analyses) was normalized in reference to the median viral loads of NC-treated wells on the first and twelfth columns for each assay plate. For each well, normalized viral loads that were either less than 0.2 or larger than 5 were considered to represent a biologically significant effect, and siRNA pools that altered intracellular viral loads in at least two out of three wells were considered as siRNA pools that alter early stages of viral infection (and thereby indirectly affect virus-induced autophagy). Six such genes were removed from the candidate list from primary screens: *ZNF224* (Entrez Gene ID: 7767), *DGAT1* (Entrez Gene ID: 8694), *NCOR2* (Entrez Gene ID: 9612), *IL20* (Entrez Gene ID: 50604), *OTUD4* (Entrez Gene ID: 54726) and *EPB41L5* (Entrez Gene ID: 57669). The remaining 310 genes were the candidate hits that pass the primary screens.

In the deconvolution screens, we performed similar analyses for each siRNA oligonucleotide as that for siRNA pools in the first analysis of the primary screens to assess the effect of each siRNA oligonucleotide on SIN-induced autophagy and HSV-1ΔBBD-induced autophagy. For each candidate gene identified by the primary screens, genes having two or more oligonucleotides passing the deconvolution screens were considered as the confirmed hits of our siRNA screens.

Bioinformatic analyses of confirmed hits from the deconvolution siRNA screens

The gene identity (Entrez gene ID) of 216 confirmed siRNA screen hits was first converted to the Universal Protein Resource (UniProt) protein knowledgebase (UniProtKB) ID using the Retrieve/ID mapping function (http://www.uniprot.org). The gene sets were then analyzed by DAVID Bioinformatics Resources 6.8 (https://david.ncifcrf.gov/) using the default settings, including molecular function (MF), biological process (BP) and cellular component (CC) categories from Gene Ontology (GOTERM), InterPro protein sequence analysis & classification (INTERPRO), the European Bioinformatics Institute (EMBL-EBI) BioCarta Pathway (BIOCARTA), Kyoto Encyclopedia of Genes and Genomes PATHWAY Database (KEGG), UniProt protein knowledgebase (UP), Online Mendelian Inheritance in Man (OMIM), The Protein Information Resource (PIR), Clusters of Orthologous Groups of proteins (COGs), Simple Modular Architecture Research Tool (SMART) and the Biological Biochemical Image Database (BBID)[48,49]. Hypergeometric tests were performed to assess the enrichment of each functional gene set for the confirmed siRNA hits. The enrichment score was defined as $-\log_{10}$(hypergeometric test *P*-value). Enriched gene sets having false discovery rate (FDR) adjusted *P*-values below 0.05 were considered as terms that were significantly enriched. All computations were conducted in the R environment version 3.5.1 (www.r-project.org).

To construct a functional enrichment network graph, the above enrichment results were plotted as a graph with nodes denoting enriched gene sets. The size of each node corresponds to the number of confirmed siRNA hits and the color intensity, which is scaled according to the enrichment score. The thickness and color intensity of lines connecting two nodes represent the extent of overlap between two gene sets, which was calculated using the following formula:

$$\text{Extent of overlap (Set A|Set B)} = \frac{\text{Number of overlapping genes}}{\text{Number of genes in Set A} + \text{Number of genes in Set B} - \text{Number of overlapping genes}}.$$

RNA interference in follow-up study of confirmed siRNA screen hits

RNA interference was performed to knock down the expression of target genes in HeLa cells cultured in either 10-cm petri dishes or 6-well plates. Cells were reverse transfected with specific siRNA oligonucleotides using Invitrogen Lipofectamine RNAiMAX according to the manufacturer's instruction for 72 h. Knockdown efficiency of target genes was confirmed by either western blot analysis or quantitative real-time PCR analysis.

Quantitative real-time PCR (qRT-PCR) analysis

Total RNA was extracted from HeLa cells using an RNeasy Plus Mini Kit (Qiagen) and further treated with DNase I (New England Biolabs) to remove residual genomic DNA contamination. Complementary DNA (cDNA) was synthesized using 1 μg purified RNA, oligo-dT primer and an iScript cDNA Synthesis Kit (Bio-Rad Laboratories). Relative gene expression levels were assessed using QuantiFast SYBR Green PCR Kit (Qiagen) on a 7500 Fast Real-Time PCR System (Applied Biosystems). The qRT-PCR primers for human *SNX32*, *SNX5*, *IFN*-β, *IFIT1* and β-*actin* (internal control) used in this study are as follows: *SNX32* forward primer, 5'-TGGCTTCCGATGAGGACCTGAA-3'; *SNX32* backward primer, 5'-CCTTGTTGGCATTCTCGTAGTCG-3'; *SNX5* forward primer, 5'-CAGAGCCCAGAGTTTTCTGTTAC-3'; *SNX5* backward primer, 5'-CCCAGCATAGTCTGTTGTTTCA-3'; *IFN*-β forward primer, 5'-ATGACCAACAAGTGTCTCCTCC-3'; *IFN*-β backward primer, 5'-GGAATCCAAGCAAGTTGTAGCTC-3'; *IFIT1* forward primer, 5'-TTGATGACGATGAAATGCCTGA-3'; *IFIT1* backward primer, 5'-CAGGTCACCAGACTCCTCAC-3'; β-*actin* forward primer, 5'-CTGGCACCCAGCACAATG-3'; β-*actin* backward primer, 5'-GCCGATCCACACGGAGTACT-3'.

Assessment of viral entry

To compare viral entry efficiency between cell lines, we used a qRT-PCR-based approach to assess relative quantity of SIN minus strand RNA and the HSV-1 immediate early gene ICP27 transcript as their levels correlate with genomic contents of incoming virions in the cytoplasm[50,51]. HeLa cells were incubated with either SIN (MOI = 50) or HSV-1ΔBBD (MOI = 25) viral inoculum (in Opti-MEM I Reduced Serum Medium) for 1 h on ice in a 4°C cold room, and then rinsed five times with ice-cold Opti-MEM I Reduced Serum Medium to remove unbound virions. Cells were either collected immediately (t = 0 h) or further cultured in fresh warm Opti-MEM I Reduced Serum Medium supplemented with 5% HI FBS for 2 h at 37°C to allow viral entry, and then collected by digestion with 0.25% trypsin-EDTA for 5 min at 37°C. RNA extraction and cDNA was performed as described above in the "Quantitative real-time PCR analysis" section. For HSV-1 infection, relative mRNA levels of viral immediate early gene *ICP27* were normalized to that of β-*actin* (internal control). For SIN infection, cDNA synthesis was performed using Invitrogen SuperScript III First-Strand Synthesis System for RT-PCR Kit (Thermo Fisher Scientific). Two sets of cDNA were made using either Oligo-dT primer or SIN minus-strand RNA-specific primer (SINmsrp), and then used to assess mRNA levels of β-*actin* (internal control) and SIN minus-strand RNA, respectively. The relative quantity of SIN minus-strand RNA was normalized to that of β-*actin* mRNA. Primers used in this assay were as follows: HSV-1 *ICP27* forward primer, 5'-GCGTCGGTCACGGCATAAGG-3'; HSV-1 *ICP27* backward primer, 5'-CGATGACTTACTGGCGGGTG-3'; SINmsrp, 5'-CTAAAGACTTGAAAGTCATAGCTG-3'; SIN forward primer, 5'-CACCCCGCACAAAAATGAC-3'; SIN backward primer, 5'-AAAAGGGCAAACAGCCAACTC-3'.

Methods for monitoring autophagy induction

To monitor autophagy in HeLa cells, we assessed LC3-I to LC3-II conversion and p62/SQSTM1 levels by western blot analyses and performed GFP-LC3, PI3P and WIPI2 fluorescence microscopy. For viral infection experiments, HeLa cells were mock-infected with Opti-MEM I Reduced Serum Medium containing 5% HI FBS (normal medium) or infected at 37°C for 1.5 h with normal media containing certain viruses at an MOI of 20 (for CVB3 and poliovirus), 10 (for CHIKV, IAV, SIN, WNV and Zika virus), and 5 (for HSV-1ΔBBD), respectively. After removal of virus-containing media, cells were cultured in fresh normal medium for an additional 3 h for fluorescence microscopic analyses or 4.5 h for western blot detection of LC3-I/II, p62/SQSTM1, ATG7, ATG13 and actin. For mTOR inhibition and nutrient-deprivation experiments, HeLa cells were cultured in normal media containing either 250 nM torin 1 or an equivalent volume of DMSO, or Earle's Balanced Salt Solution (EBSS, Thermo Fisher Scientific) for 1 h at 37°C. To monitor autophagic flux, bafilomycin A1 (final concentration 100 nM), a lysosomal inhibitor, was added to culture media at 1 h prior to fixation (in fluorescence microscopy experiments) or 2 h prior to cell collection (in western blot experiments).

Fluorescence microscopy and image analyses

HeLa cells on Nunc Lab-Tek II 4-well glass chamber slides (Thermo Fisher Scientific) were quickly rinsed once with cold DPBS containing Ca^{2+} and Mg^{2+} (DPBS-CaMg; Sigma-Aldrich) and then fixed with 3% PFA in DPBS-CaMg for 10 min at room temperature. After removal of the fixative, cells were rinsed once with DPBS-CaMg. For GFP-LC3 fluorescence microscopy using HeLa/GFP-LC3 cells, slides were directly mounted with VECTASHIELD Antifade Mounting Medium with DAPI (Vector Laboratories H-1200) and stored at 4°C until imaging. For immunofluorescence microscopy using HeLa cells, cells were permeabilized in 0.2% saponin in DPBS (Sigma-Aldrich D8537) for 15 min at room temperature and then incubated with blocking buffer (DPBS containing 1% BSA and 0.1% saponin) for an additional 30 min. HeLa cells were stained with primary antibodies for 1 h at room temperature and rinsed three times with DPBS. HeLa cells were then incubated with Alexa Fluor secondary antibodies for 1 h at room temperature, rinsed five times with DPBS, mounted with VECTASHIELD Antifade Mounting Medium with DAPI (Vector Laboratories H-1200) or ProLong Diamond Antifade Mountant with DAPI (Thermo Fisher Scientific P36961) and stored at 4°C until imaging. For PI3P fluorescence microscopy, HeLa cells were fixed with 4% PFA in DPBS-CaMg for 20 min at room temperature followed by a single quick wash with DMEM. Cells were permeabilized with DPBS containing 0.1% N-lauroylsarcosine sodium (Sigma-Aldrich L9150) and 2% BSA for 5 min, and then incubated with a PI3P-specific fluorescent probe PX-Alexa555[28,52] for 15 min. After washing with DPBS containing 2% BSA twice, slides were mounted with ProLong Diamond Antifade Mountant with DAPI and stored at 4°C until imaging. To minimize fluorescent signal decay, slides were imaged on the second day after mounting.

Fluorescent micrographs were acquired using a Zeiss Axio Imager Z2 microscope equipped with a Photometrics CoolSnap HQ2 CCD camera using a Zeiss PLAN APOCHROMAT 20X/0.8 NA wide-field objective or PLAN APOCHROMAT 40X/0.9 NA oil immersion objective. Z-stack images were acquired with the same acquisition times (for each primary

antibody) for samples prepared in each batch of experiment. Z-stack images were deconvolved with AutoQuant version X2 (Media Cybernetics) and further analyzed with Imaris version 9.3.0 (Bitplane Inc.) using the same settings for each batch of samples. Background thresholding using secondary antibody control staining was applied for all experiments. Random images were chosen from greater than 100 cells per well of triplicate samples for each condition for analysis by an observer blinded to experimental condition.

Acid bypass assay

To determine whether viral entry at the plasma membrane triggers autophagy, HeLa/GFP-LC3 cells in Nunc Lab-Tek II 4-well glass chamber slides were rinsed once with ice-cold Opti-MEM I Reduced Serum Medium (Opti-MEM) and incubated in ice-cold Opti-MEM on ice for 10 min in a 4°C cold room. Cells were then incubated in virus-free ice-cold Opti-MEM (mock infection) or ice-cold Opti-MEM containing SIN (strain SVIA, MOI = 50) or HSV-1ΔBBD (MOI = 25) on ice in a 4°C cold room for 1 h to allow viral attachment to cell surface. After discarding viral inocula, cells were rinsed three times with ice-cold Opti-MEM to remove unbound virions. Cells were then incubated with ice-cold Opti-MEM (pH 7.4) or acidic Opti-MEM (pH 5.4) for 10 min at 4°C. The pulse of acidic treatment leads to fusion between the viral envelope and cellular plasma membrane, and thus viral entry occurs at the plasma membrane instead of conventional endolysosomal routes (which is therefore called an “acid bypass”). The medium was replaced with warm fresh Opti-MEM supplemented with 5% HI FBS (normal medium) and cells were cultured for 2 h at 37°C (to allow viral entry in the control group without acid bypass treatment). The medium was replaced with warm fresh normal medium and cells were further cultured for an additional 2.5 h at 37°C. GFP-LC3 fluorescence microscopy was performed as described in the section “Fluorescence microscopy and image analyses”. To compare viral entry efficiency in HeLa cells receiving the two types of pulse treatments (pH 5.4 versus pH 7.4), viral infection was performed similarly as described above except that cells were collected at the end of 2-hour culture at 37°C (without medium change and without an additional 2.5-hour culture). Viral entry efficiency was then examined similarly as described in the section “Assessment of viral entry”.

Assessment of bacterial xenophagy

To study autophagic capture of Group A *Streptococcus* (xenophagy), Group A *Streptococcus* was grown to mid-log phase and collected by centrifugation at 3,000 g for 5 min. Bacterial pellets were rinsed three times with Opti-MEM I Reduced Serum Medium (Opti-MEM). The OD_{600} of bacteria resuspended in Opti-MEM was determined using a GENESYS 30 Visible Spectrophotometer (Thermo Fisher Scientific) and the number of viable bacteria (colony-forming unit [cfu]) was determined on Blood Agar (TSA with 5% Sheep Blood) Plates (Thermo Fisher Scientific). To infect wild-type and $SNX5^{KO}$ HeLa/GFP-LC3 cells, cells were incubated with antibiotic-free Opti-MEM supplemented with 5% FBS containing Group A *Streptococcus* (at an MOI of 50) for 1 h at 37°C. Cells were washed two times with Opti-MEM to remove unbound bacteria, and then cultured in fresh Opti-MEM supplemented with 5% FBS and antibiotics (100 μg/ml gentamicin and 100 U/ml penicillin G, which kill the extracellular bacteria) for an additional three hours at 37°C. Cells were then fixed for

fluorescence microscopy analysis as described in the section “Fluorescence microscopy and image analyses”.

Endolysosomal LC3 lipidation induced by osmotic imbalance

Wild-type and *SNX5*^{KO} HeLa/GFP-LC3 cells were cultured in Opti-MEM I Reduced Serum Medium supplemented with 5% FBS (normal medium) in Nunc Lab-Tek II 4-well glass chamber slides overnight. Hypotonic medium was made by mixing fresh normal medium with sterile water (Sigma-Aldrich W4502) at a ratio of 20:80 (vol/vol). Cells were rinsed three times with DPBS (Sigma-Aldrich D8537) and then cultured in fresh normal medium or hypotonic medium for 1 h. Cells were fixed and immunofluorescence microscopy was performed using the protocol described in the section “Fluorescence microscopy and image analyses” and stained for the early endosomal marker EEA1 and the lysosomal marker LAMP1.

Monensin-driven LC3-associated phagocytosis of latex beads

Wild-type and *SNX5*^{KO} HeLa/GFP-LC3 cells (80,000 cells/well) were cultured in Opti-MEM I Reduced Serum Medium supplemented with 5% FBS (normal medium) in Nunc Lab-Tek II CC2 4-well glass chamber slides (Thermo Fisher Scientific) overnight. Polybead Microspheres (3.00 μm in diameter) (Polysciences Inc. 17134-15) were washed twice by resuspending the beads in sterile PBS and pelleting for 5 min at 2,500 g. Cells were incubated with fresh normal medium containing beads (approximately 50 beads per cells) for 4 h. Cells were rinsed three times with sterile PBS to remove unengulfed beads and cultured for 45 min in fresh normal medium containing 100M monensin or an equivalent volume of solvent control (ethanol). Cells were rinsed twice with cold PBS and then fixed in ice-cold methanol for 4 min in −20°C. Cells were rinsed twice with PBS and blocked in PBS containing 2% BSA (blocking buffer) for 30 min at room temperature. Cells were incubated with blocking buffer containing goat anti-LAMP1 polyclonal antibody for 1 h at room temperature. Cells were rinsed three times in PBS, and then incubated with blocking buffer containing Alexa Fluor 594 secondary antibody for 1 h at room temperature. Cells were rinsed five times with PBS and slides were mounted with ProLong Diamond Antifade Mountant with DAPI and stored at 4°C until imaging. Intracellular structures containing latex beads were studied with immunofluorescence microscopy and differential interference contrast (DIC) microscopy (also known as Nomarski interference contrast microscopy).

Glucose transporter 1 (GLUT1) lysosomal sorting assay

Retromer activity was monitored by a GLUT1 lysosomal sorting assay as previously described[53], in which lysosomal localization of mis-sorted GLUT1 serves as an indicator of defective retromer activity. HeLa cells were transfected with NC control siRNAs or siRNAs targeting *SNX5*, *SNX32*, *VPS29* and *ATG7* for 72 h. Immunofluorescence microscopy was performed using the protocol described in the section “Fluorescence microscopy and image analyses” with staining for GLUT1 and LAMP1. Quantitative analyses of colocalization between GLUT1 and LAMP1 (Manders’ overlap coefficient) were performed using the ImarisColoc module of Imaris version 9.3.0 (Bitplane Inc.).

Transferrin receptor recycling assay

To assess the fast and slow recycling activity of plasma membrane-anchored receptors through endocytic pathways in HeLa cells, a pulse-chase transferrin receptor recycling assay was performed as follows. Wild-type and *SNX5*^{KO} HeLa cells (12,000 cells/well) were seeded in 96-well stripwell plates (Corning) at 80% confluency one day prior to the experiment. Cells were first rinsed three times with 200 μL assay buffer PBS^{4+} (PBS supplemented with 1 mM $CaCl_2$, 1 mM $MgCl_2$, 0.2% BSA and 5 mM D-glucose) and then cultured in 100 μL PBS^{4+} for 30 min at 37°C to minimize the background biotin signal. Cells were chilled down in 100 μL ice-cold PBS^{4+} on ice in a 4°C cold room for 5 min, and then incubated with 100 μL PBS^{4+} (blank controls) or PBS^{4+} containing 5 μg/mL Biotin-transferrin (Biotin-Tfn) (Sigma-Aldrich T3915). The blank controls were left on ice until fixation. Biotin-Tfn-treated cells were cultured at 37°C for either 10 min or 30 min to allow uptake of Biotin-Tfn into cells, which corresponds to the assessment of fast recycling pathway or slow recycling pathway, respectively. Biotin-Tfn uptake was stopped by replacing the buffer with 200 μL fresh ice-cold PBS^{4+} and cells were rapidly cooled on ice. Cells were rinsed once with ice-cold PBS^{4+} to remove excess of unbound Biotin-Tfn in wells. Cells were then treated with avidin and biocytin to mask surface bound Biotin-Tfn as follows. First, cells were incubated in 50 μL ice-cold PBS^{4+} containing 50 μg/mL Invitrogen avidin (Thermo Fisher Scientific 434401) on ice for 10 min. Cells were rinsed twice with ice-cold PBS^{4+}, and then incubated in 50 μL ice-cold PBS^{4+} containing 5 μg/mL Invitrogen biocytin (Thermo Fisher Scientific B1592) on ice for 15 min to mask cell surface-bound Biotin-Tfn. Cells were rinsed twice with ice-cold PBS^{4+}, and one strip of cells was temporarily stored on ice until fixation, which served as the “initial total intracellular Biotin-Tfn content” controls (i.e. t = 0 min) for the following chase steps. The remaining strips of cells were cultured in 100 μL PBS^{4+} containing 2 mg/mL (saturation concentration) holo-transferrin (Sigma-Aldrich T4132) at 37°C for serial chase times (2.5, 5, 10, 20 and 30 min) to allow recycling of endosomal biotin-Tfn-bound Tfn receptor to the cell surface. To stop the recycling, the buffer was replaced with 100 μL fresh ice-cold PBS^{4+}. Cells were further rapidly rinsed three times with 200 μL ice-cold wash buffer (200 mM acetic acid, 200 mM NaCl, pH 2.3) for 15 sec each wash to remove plasma membrane-associated Biotin-Tfn. All strips of cells were rinsed three times with 200 μL ice-cold PBS, and fixed in 100 μL 4% PFA in PBS for 30 min at 37°C. Cells were rinsed three times with 200 μL ice-cold PBS, and permeabilized in PBS containing 0.1% Triton X-100 for 5 min at room temperature. Cells were blocked with casein blocking buffer (Sigma-Aldrich B6429) for an additional 30 min at room temperature. Cells were incubated with 200 μL Q-PBS buffer (pH 7.4) containing 2% BSA, 0.1% lysine, 0.01% saponin and streptavidin-HRP (Roche; 1:10,000) for 1 h. Cells were rinsed six times with 200 μL PBS for 5 min each wash, and incubated with 200 μL o-phenylenediamine dihydrochloride (OPD) solution (Sigma-Aldrich) for 20 min. Reactions were stopped by adding 50 μL 5M H_2SO_4 solution. Absorbance at 490 nm and 650 nm was determined using a Synergy H1 Hybrid Multi-Mode Reader (BioTek Instruments). To determine the total protein levels in each well, cells were rinsed five times with 200 μL PBS, and then incubated with 100 μL Pierce BCA Solution (Thermo Fisher Scientific) on a shaker for 30 min at 60°C. Absorbance at 562 nm was determined using a Synergy H1 Hybrid Multi-Mode Reader (BioTek Instruments). HRP activity was normalized to protein concentration for each well. The percentage of remaining intracellular Biotin-Tfn

content for each chase time point was calculated in reference to the initial total intracellular Biotin-Tfn content.

Epidermal growth factor receptor (EGFR) endolysosomal degradation assay

Endolysosomal function of HeLa cells was assessed by an epidermal growth factor (EGF)-induced EGFR endolysosomal degradation assay. HeLa cells (180,000 cells/well in 6-well plates) were cultured overnight in DMEM supplemented with 10% FBS, 100 units/mL penicillin and 100 μg/mL streptomycin. Cells were then starved for 16 h in serum-free DMEM and treated with DMEM containing 30g/mL cycloheximide for 30 min to suppress protein synthesis. Cells were stimulated with 100 ng/mL EGF (Thermo Fisher Scientific PHG0313), and collected at 0, 0.5, 1, 2 and 4 h, respectively. EGFR and actin protein levels were analyzed by western blot analysis. Western blot images were collected using a G:Box Chemi Gel Doc System (Syngene) and densitometry analysis of protein bands was performed using the software GeneTools version 4.3.10.0 (Syngene). Relative EGFR protein levels were normalized to corresponding actin controls and then converted to percentage values in reference to unstimulated cells (t = 0 h).

Viral infectivity assays and viral growth curves

Viral infection in cultured cells was examined by viral infectivity assays, multi-step growth curves and single-step growth curves. For the viral infectivity assay, HeLa cells were seeded in 12-well plates (100,000 cells per well) in Opti-MEM I Reduced Serum Medium supplemented with 5% HI FBS (normal medium) one day prior to infection. Confluent cell monolayers were incubated with 2-fold serially diluted viral inoculum in normal medium for 1.5 h. After removal of viral inocula, cells were cultured in 1× MEM supplemented with 1% HI FBS and 1% methylcellulose (Sigma-Aldrich M0512) for 3 days. Cell monolayers were fixed in methanol for 15 min at room temperature and then stained in 1× crystal violet solution (containing 0.5% crystal violet and 25% methanol). The numbers of plaques on cell monolayers correspond to the numbers of cells that established infection during primary infection with viral inoculum, as methylcellulose blocks viral spread through culture medium without affecting viral direct cell-to-cell transmission. Thus, plaque numbers normalized to viral input for each well indicate the relative magnitude of cellular susceptibility to viral infection (i.e. viral infectivity) for each cell line.

To assess viral multi-step growth and single-step growth in HeLa cells, cell monolayers were infected with viral inoculum in Opti-MEM I Reduced Serum Medium supplemented with 5% HI FBS (normal medium) at MOI of 0.01 and 10 for 1.5 h, respectively. After removal of viral inocula, cells were cultured in fresh normal medium for up to 6 days. Viral multi-step growth in primary MEFs were assessed similarly as described above, except that MEFs were cultured using DMEM supplemented with 10% HI FBS. Viral titers at selected time points were determined by plaque assay.

Co-immunoprecipitation (co-IP)

To investigate the interaction between endogenous proteins, HeLa cells were treated with PIK-III (5 μM) or DMSO for 1 h. HeLa cells were lysed in ice-cold 1× lysis buffer (pH 7.5) containing 50 mM HEPES, 150 mM NaCl, 1 mM EDTA, 10% glycerol, 1% Triton X-100,

cOmplete proteinase inhibitor cocktail (Roche) and Halt phosphatase inhibitor cocktail (Thermo Fisher Scientific) on ice for 30 min, and further homogenized by passage through 18-gauge needles fitted onto sterile plastic syringes fifteen times. The insoluble fraction of cell lysates was removed by centrifugation at 10,000 g and 4°C for 15 min. Cell lysates were further cleared by incubation with 10L Protein G PLUS-agarose beads (Santa Cruz Biotechnology) for 30 min at 4°C followed by centrifugation at 1,000 g and 4°C for 1 min. The total protein concentration of supernatants was determined using a Quick Start Bradford Protein Assay Kit (Bio-Rad Laboratories), and adjusted to the same concentration by adding 1× lysis buffer. Cell lysates (equivalent volume for each experimental group) were incubated with anti-beclin 1 and anti-SNX5 antibodies or an appropriate control IgG for 3 h at room temperature, and then subjected to immunoprecipitation by the addition of 25L Protein G PLUS-Agarose beads (Santa Cruz Biotechnology) for 1 h at room temperature. Agarose beads were pelleted by centrifugation at 1,000 g and 4°C for 1 min and washed five times with ice-cold 1× lysis buffer. Immunoprecipitates were eluted by boiling agarose beads in 2× Laemmli sample buffer (Bio-Rad Laboratories) containing 5% β-mercaptoethanol (Bio-Rad Laboratories) for 5 min and then analyzed by western blot.

Western blot analyses

HeLa cell lysates were prepared by incubating cells with ice-cold 1× lysis buffer (pH 7.5) containing 50 mM HEPES, 150 mM NaCl, 1 mM EDTA, 10% glycerol, 1% Triton X-100, cOmplete proteinase inhibitor cocktail (Roche) and Halt phosphatase inhibitor cocktail (Thermo Fisher Scientific) on ice for 30 min. Cell lysates were then centrifuged at 10,000 g and 4°C for 15 min to remove the insoluble fraction. The supernatant was then mixed with an equal volume of 2× Laemmli sample buffer (Bio-Rad Laboratories) containing 5% β-mercaptoethanol (Bio-Rad Laboratories) and boiled for 5 min. Denatured proteins were separated by SDS-PAGE using 4-20% Mini-PROTEAN TGX precast protein gels (Bio-Rad Laboratories) and transferred to Immun-Blot PVDF membranes (Bio-Rad Laboratories). Membranes were blocked with blotting-grade blocker (Bio-Rad Laboratories) or 2% BSA in 1× PBS buffer containing 0.05% Tween 20 (PBST), incubated with primary and secondary antibodies diluted according to manufacturers' instructions, and washed five times with 1× PBST. Protein bands were visualized with SuperSignal West Pico PLUS Chemiluminescent Substrate (Thermo Fisher Scientific) on a BioSpectrum imaging system (Ultra-Violet Products) or Light Labs Ultra Blue X-ray film (Light Labs). Densitometry analysis of protein bands was performed using the software Multi Gauge 3.0 (FUJIFILM). Relative protein levels were normalized to according actin controls. To further validate that viral infection induces degradation of p62/SQSTM1 instead of its translocation into the Trion X-100-insoluble fraction, HeLa cells were also lysed in RIPA buffer (Cell Signaling Technology) containing 1% SDS after mock or viral infection. Western blot and densitometry analyses were performed similarly as described above.

Expression and purification of Class III phosphatidylinositol 3-kinase (PI3KC3) complexes

PI3KC3 complexes were prepared using a mammalian expression system from a suspension culture of HEK293F cells. Expression plasmids for PI3KC3 complex components include pCAG-OSF-ATG14 for Strep-Flag tagged human ATG14, pCAG-OSF-UVRAG for Strep-Flag tagged human UVRAG, pCAG-NT-P150 for human VPS15 (also known as p150),

pCAG-NT-VPS34 for VPS34 (also known as PI3KC3 or PIK3C3), and pCAG-NT-beclin1 for beclin 1[54]. To obtain PI3KC3-C1 complexes (containing ATG14, VPS15, VPS34 and beclin 1) and PI3KC3-C2 complexes (containing UVRAG, VPS15, VPS34 and beclin 1), two plasmid cocktails (0.5 mg per plasmid per 1 L culture medium), were respectively transfected into HEK293F cells (when cell density reached 1,000,000 cells/mL) using polyethylenimine (PEI) at the mass ratio 1.5:1 (PEI:plasmids). HEK293F cells were cultured in a 37°C incubator with a humidified atmosphere with 8% CO_2 in air on an orbital shaker rotating at 120 rpm for three days.

For purification of PI3KC3 complexes, HEK293F cells were collected at 72 h after transfection by centrifugation at 400 g and 4°C for 20 min. Cell pellets were then lysed in ice-cold 1× lysis buffer containing 20 mM Tris-HCl (pH 8.0), 150 mM NaCl, 1 mM dithiothreitol (DTT), 1% Triton X-100 and protease inhibitor cocktail (Roche) on ice for 10 min. After centrifugation at 13,000 g and 4°C for 30 min, the supernatant was filtrated through a 0.45-μm filter (Roche). Precleared supernatant was incubated with StrepTactin Sepharose High Performance resin (GE Healthcare) for 1 h at 4°C. The resin was carefully washed three times with ice-cold washing buffer containing 100 mM Tris-HCl (pH 8.0), 300 mM NaCl and 1 mM DTT. PI3KC3 complexes were eluted with 10 mM desthiobiotin (Sigma-Aldrich) and concentrated by centrifugation using Amicon Ultra-15 Centrifugal Filter Units 100K (EMD Millipore) at 4°C. Concentrated eluate was further purified by gel filtration using Superose 6 Increase 3.2/300 pre-packed high performance glass columns (GE Healthcare) at 4°C, which were equilibrated with the gel filtration buffer containing 20 mM Tris-HCl (pH 8.0), 150 mM NaCl and 1 mM DTT. PI3KC3 complex peak fractions were combined and stored in small aliquots at −80°C after being snap-frozen in liquid nitrogen. The concentration of PI3KC3 complex eluates was quantitated using the protein A280 method. The purity of protein complexes was examined by SDS-PAGE and Coomassie blue staining using GelCode Blue Safe Protein Stain (Thermo Fisher Scientific 24594) according to the manufacturer's instruction.

Amino Acid Sequence Alignment and Secondary Structure Prediction of SNX5 and Closely-related Sorting Nexins

Amino acid sequence of nine vertebrate SNX5 homologs and four closely-related human sorting nexins (SNX1, SNX2, SNX6 and SNX32) were acquired form National Center for Biotechnology Information (NCBI) Reference Sequences (RefSeq) database. Their NCBI accession IDs are as follows: zebrafish snx5, NP_999934; frog snx5, NP_001016081; snake SNX5, XP_025024423; Lizard snx5, XP_003219930; chick SNX5, NP_001006178; mouse Snx5, NP_001186117; pig SNX5, XP_020933988; chimpanzee SNX5, XP_016792968; human SNX5, NP_689413; human SNX1, NP_003090; human SNX2, NP_003091; human SNX6, NP_689419; human SNX32, NP_689973. Amino acid sequence alignment of proteins was performed using Cluster Omega (https://www.ebi.ac.uk/Tools/msa/clustalo/). Protein secondary structure prediction was performed using the University College London (UCL) PSIPRED Protein Sequence Analysis Workbench (http://bioinf.cs.ucl.ac.uk/psipred/).

Expression and purification of recombinant SNX5 proteins

Wild-type SNX5 and a mutant SNX5 EEE (that carries triple mutations K328E/R330E/K332E) were prepared using a bacterial expression system. The coding region of SNX5 and SNX5 EEE were cloned into BamHI/SalI sites of the ppSUMO vector, a modified pET-28a vector that contains an N-terminal hexa-histidine-tag followed by a SUMO-tag and a recognition site for SUMO protease, Ulp. The empty vector and SNX5 plasmids were transformed into the chemically competent *E. coli* strain BL21(DE3) and grown to an optical density at a wavelength of 600 nm (OD_{600}) of 0.8 in 2× YT medium. Protein expression was induced by addition of 0.2 mM isopropyl-β-D-thiogalactopyranoside (IPTG) followed by overnight culture at 16°C. Cells were lysed in 1× bacterial lysis buffer containing 20 mM Tris (pH 8.0), 500 mM NaCl, and 2 mM β-mercaptoethanol by French pressing using Emulsiflex-C5 (AVESTIN). Cell lysates were cleared by centrifugation at 15,000 g and 4°C for 1 h. Proteins in the lysates were purified using 1 mL HisTrap columns (GE Healthcare) and size exclusion chromatography using Superdex 200 increase 10/300 gel filtration columns (GE Healthcare) equilibrated with a buffer containing 20 mM Tris (pH 8.0), 150 mM NaCl, and 2 mM DTT. SUMO control, SUMO-SNX5 and SUMO-SNX5 EEE were further concentrated by centrifugation using Amicon Ultra-15 Centrifugal Filter Units 10K (EMD Millipore) and stored in small aliquots at −80°C after being snap-frozen in liquid nitrogen. Protein concentration and quality was assessed as described above. Approximately 0.1 nanomole of SUMO control, SUMO-SNX5 and SUMO-SNX5 EEE was loaded per lane on an SDS-PAGE gel.

In vitro binding assay

To determine whether SNX5 directly binds PI3KC3-C1 or PI3KC3-C2 complexes, 0.2 nanomole of bacterially-purified SUMO control, SUMO-SNX5 and SUMO-SNX5 EEE were incubated with PI3KC3-C1 or PI3KC3-C2 complexes on Strep-Tactin resin or empty resin in 1× binding buffer containing 20 mM Tris-HCl (pH 8.0), 150 mM NaCl, 1 mM DTT, 1% Triton X-100 and protease inhibitor cocktail (Roche) for 3 h at room temperature. Strep-Tactin resin was pelleted by centrifugation at 1,000 g for 1 min and washed six times with ice-cold 1× binding buffer. Captured protein complexes were eluted by boiling resin in 2× Laemmli sample buffer (Bio-Rad Laboratories) containing 5% β-mercaptoethanol (Bio-Rad Laboratories) for 5 min and then analyzed by western blot.

Liposome preparation

The lipid substrate for the *in vitro* lipid kinase assay was phosphatidylinositol (PI) incorporated on Large Unilamellar Vesicles prepared by Extrusion Technique (LUVETs)[29,30] using a lipid mixture that resembles endosomal lipid composition[31,32]. PI-containing liposomes were composed of 47.5% porcine brain phosphatidylcholine (PC, Avanti Polar Lipids 840053), 23% porcine brain phosphatidylethanolamine (PE, Avanti Polar Lipids 840022), 10% bovine liver PI (Avanti Polar Lipids 840042), 9% porcine brain sphingomyelin (SM, Avanti Polar Lipids 860062), 8.5% porcine brain phosphatidylserine (PS, Avanti Polar Lipids 840032), and 2% protonated phosphatidylinositol 4,5-bisphosphate (PI[4,5]P_2, Avanti Polar Lipids 840046). PI-free control liposomes were composed of similar lipid composition except that PI was replaced with PS. Six mM of lipid components

were mixed together in 1:1 (vol/vol) chloroform:methanol and dried in glass tubes under a stream of nitrogen. The lipid film was further vacuum-dried for 2 h at room temperature and then rehydrated into 1× liposome buffer containing 20 mM Tris-HCl (pH7.5), 150 mM NaCl and 1 mM DTT. Lipids were subjected to ten cycles of freeze and thaw between liquid nitrogen and a 42°C water bath, and then extruded twenty-one times through polycarbonate filters with pore sizes of 100 nm or 30 nm in diameter (Avanti Polar Lipids). These LUVETs of two sizes are respectively designated as “larger” and “smaller” liposomes in this study. Liposomes were stored in glass vials at 4°C and used for *in vitro* lipid kinase assay within 24 h.

In vitro lipid kinase assays

The kinase reactions were performed in 8-tube strip PCR tubes at a ratio of 1:1:1 (vol/vol/vol) for PI-containing or PI-free liposomes (2 mM of total lipids) (1/3 volume), purified PI3KC3-C1 and varying concentrations of SNX5 diluted in 1× liposome buffer (1/3 volume) and a kinase reaction buffer containing ATP (1/3 volume; added at the last step to initiate the reaction). The kinase reaction buffer consisted of 20 mM Tris-HCl (pH7.5), 105 mM NaCl, 30 mM $MgCl_2$, 1 mM DTT and 300 μM ATP, which has the same osmotic pressure as the 1× liposome buffer. The reactions were carried out for 30 min at 37°C. ATP consumption in each reaction was assessed using an ADP-Glo Kinase Assay Kit (Promega).

Cryogenic electron microscopy (cryo-EM) and assessment of liposomal curvature

To investigate SNX5-induced liposomal deformation, the “larger” LUVETs (extrusion filter pore size: 100 nm in diameter) containing 2 mM total lipids were incubated with 800 nM of SUMO control, SUMO-SNX5 and SUMO-SNX5 EEE in 1× liposome buffer (without PI3KC3-C1 and ATP) for 30 min at 37°C. Lacey Carbon film 300 mesh Copper grids (Agar Scientific AGS166-3) were glow-discharged at 30 mA for 40 seconds in a Pelco easiGlow Glow Discharge Cleaning System (Ted Pella). A drop (3.5 μL) of the suspension was then applied onto the carbon-coated side of a specimen grid held by forceps in the blotting position inside the environmental chamber (humidity 100%) of FEI Vitrobot (Thermo Fisher Scientific) at room temperature. Grids were immediately blotted at a force of 12 for 4 seconds, plunged into the liquid ethane, and then stored in liquid nitrogen until imaging. The specimens were examined in liquid nitrogen using an FEI Talos Arctica TEM (Thermo Fisher Scientific). Micrograph were collected at a magnification of 28,000 under 300 kV and low-dose condition (approximately 20 $e^{-}/Å^2$) using an FEI Eagle 4k × 4k CCD.

In cryo-EM micrographs, liposomes display in the form of either circular or elliptical shapes (in two-dimensional space), which correlate with spherical and ellipsoid shapes of the liposome (in three-dimensional space). For each experimental group, the lengths of the major axis (2a) and minor axis (2b) of an ellipse were quantitated for at least 150 liposomes per condition. Since the circle can be considered as a unique ellipse with two foci at the same spot (the center), 2a is equal to 2b for a circle. Unlike a constant curvature along the circle, an ellipse has continuously altering curvature with the highest curvature seen at two vertex points. In differential geometry, the radius of curvature (R), which is the reciprocal of

the curvature (κ), inversely correlates with the magnitude of curvature. The radius of curvature at vertex points of an ellipse was quantitated and compared between experimental groups.

Animal studies

Animal studies were performed in a barrier facility at the University of Texas Southwestern Medical Center. Mice were raised under the following housing conditions: ambient temperature, 70°F to 75°F; humidity, 30% to 50%; normal light-dark cycle (lights on 6 a.m. and lights off 6 p.m.); chow, Teklad Global 16% Protein Rodent Diet (Envigo 2916); water, reverse osmosis water. For *in vivo* studies, intracerebral (i.c.) infection was performed for HSV-1, SIN and WNV, and subcutaneous infection was performed for CHIKV. All intracerebral infections were performed by injecting virus diluted in 30 μL Hank's Balanced Salt Solution (HBSS, Thermo Fisher Scientific) in the right cerebral hemisphere. For HSV-1 infection, eight- to ten-week-old littermate *Snx5*$^{+/+}$ and *Snx5*$^{-/-}$ mice were infected i.c. with 50,000 plaque-forming units (pfu) of HSV-1ΔBBD or HSV-1ΔBBD-MR. Since HSV-1ΔBBD-MR is significantly more virulent than HSV-1ΔBBD, this strain was also administrated using a lower dose (500 pfu, i.c.) to ensure that differences observed between *Snx5*$^{+/+}$ and *Snx5*$^{-/-}$ mice in susceptibility to infection with HSV-1ΔBBD is truly specific for HSV-1 strains that lack the ability to inhibit host autophagy. For SIN infection, seven-day-old *Snx5*$^{+/+}$ and *Snx5*$^{-/-}$ neonatal mice were infected i.c. with 1,000 pfu of SIN strains dsTE12Q or dsTE12Q.dnAtg5 (SIN.dnAtg5). For WNV infection, 5.5-day-old *Snx5*$^{+/+}$ and *Snx5*$^{-/-}$ neonatal mice were infected i.c. with 1 pfu of WNV strain Egypt-101. For infection with CHIKV, seven-day-old *Snx5*$^{+/+}$ and *Snx5*$^{-/-}$ neonatal mice were infected subcutaneously with 100,000 pfu of CHIKV strain 06-021 in 30 μL HBSS. All mice were monitored daily. Infected animals were randomly chosen for tissue collection at designated time points post infection. To assess viral loads in mouse brains, 10% (weight/volume) homogenates of the right hemispheres were prepared by grinding brains in HBSS followed by either three freeze-thaw cycles (for HSV-1) or no freeze-thaw cycle (SIN), and then assessed by plaque assay titration. For histopathology studies, the left hemispheres were fixed in 4% PFA, embedded in paraffin, and further analyzed by immunohistochemistry assays as described below. For mortality studies, mice that survived from viral infection were euthanized on day 21 post infection. Since the *in vivo* virulence of SIN.dnAtg5 is much lower than the parental strain dsTE12Q, SIN.dnAtg5-infected mice were monitored until day 28 post infection and all surviving mice were euthanized at the end of the experiment. All animal procedures were performed in accordance with institutional guidelines and with approval from the Institutional Animal Care and Use Committee of the University of Texas Southwestern Medical Center.

Histology

Five-μm-thick sagittal sections of mouse brain were prepared using PFA-fixed and paraffin-embedded samples. Terminal deoxynucleotidyl transferase dUTP nick end labeling (TUNEL) staining of mouse brain sections was performed using Apoptag Peroxidase In Situ Apoptosis Detection Kit (EMD Millipore) and SIGMA*FAST* 3,3'-diaminobenzidine tablets (DAB; Sigma-Aldrich) according to the manufacturers' instructions. High-resolution montages of the entire sagittally sectioned mouse brain slides were acquired using a Zeiss

Axio Scan.Z1 slide scanner equipped with a Zeiss PLAN APOCHROMAT 20X/0.8 NA objective (Carl Zeiss Microscopy), and then analyzed with NDP.view version 2.3.13 (Hamamatsu Photonics). The number of TUNEL-positive foci per mouse brain sections was determined by an observer blinded to experimental condition.

Statistical analyses

Statistical analyses for genome-wide siRNA screens are described in the section "High-content image-based genome-wide siRNA screens". Where appropriate, two-sided statistical tests were used throughout this study. For Kaplan-Meier survival curves in animal studies, log-rank tests (two-sided) were performed using the software Prism 8 version 8.3.0 (GraphPad Software). For *in vivo* pathogenesis analysis and all the *in vitro* assays, *P* values were determined using the open-source R software package version 3.6.2 (www.r-project.org). Unpaired two-tailed *t*-tests were used for comparisons of two means, and one-way ANOVA analysis with Dunnett's test for multiple comparisons was performed to assess the significance of multiple experimental groups versus a control condition. Two-way ANOVA analysis was performed to assess the significance of the interaction of two independent variables. Linear regression analysis was used to assess the dose-dependent effect of a variable, and two- or three-way interaction terms in these linear models were then used to determine the significance of differences of dose-dependent effects between different treatment groups.

Data availability

All relevant data supporting the findings of this study are available within the manuscript and its supplementary information files. All figures, including Figs. 1 - 3 and Extended Data Figs. 1, 3 - 10 have associated raw data. Original blots are available in Supplementary Fig. 1. Original protein sequences were acquired from the NCBI RefSeq database, and the link to this database and protein accession numbers are provided in the Amino Acid Sequence Alignment section of the Methods.

Code availability

Custom codes (for R packages) used in siRNA screen analyses are available from the GitHub database (https://github.com/xiao-zang/snx5).

Extended Data

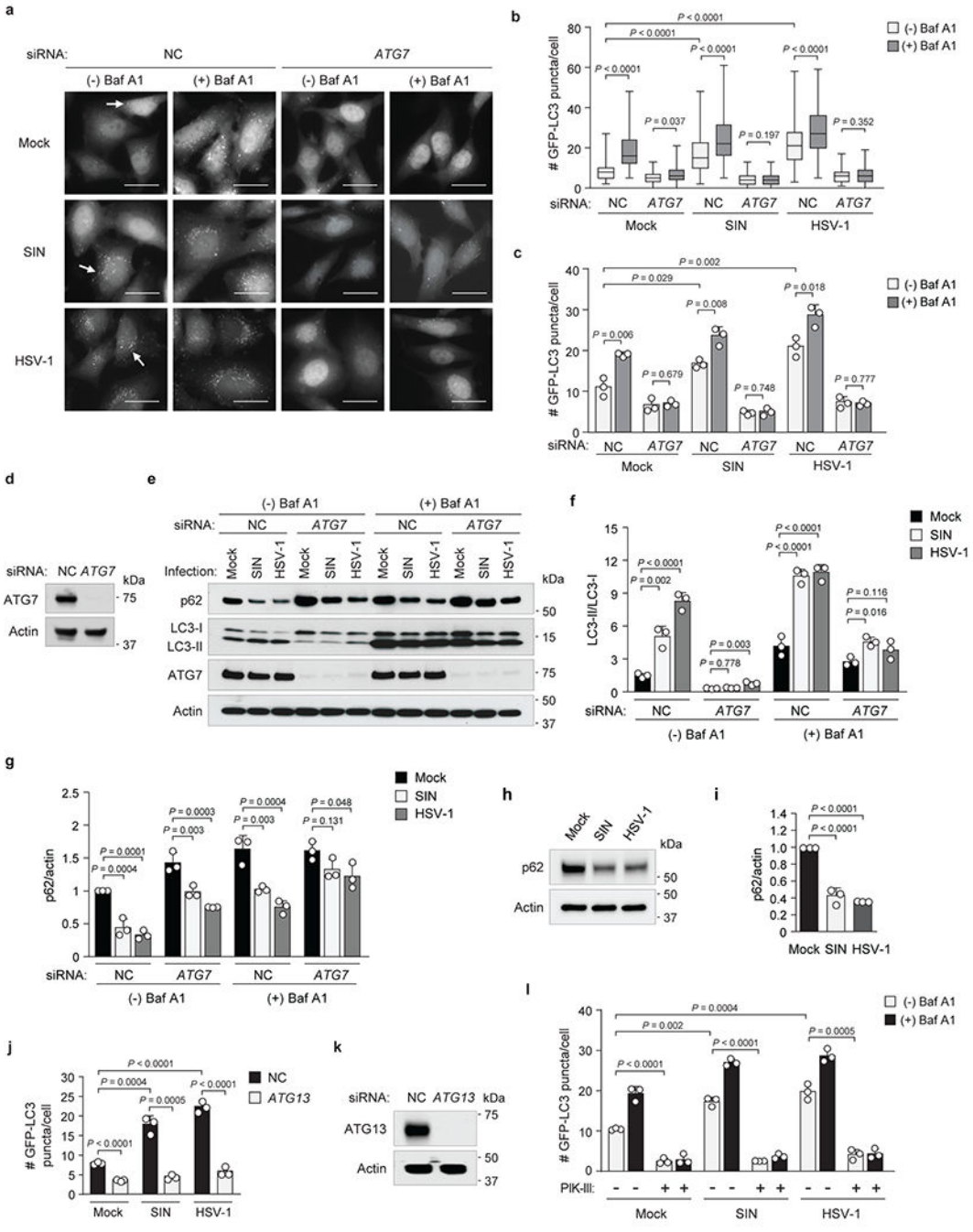

Extended Data Fig. 1. SIN and HSV-1ΔBBD increase autophagy in HeLa cells via an ATG7-, ATG13-, and PI3KC3-dependent mechanism.

a-c, Representative fluorescent micrographs (**a**) and quantitation (**b**, **c**) of GFP-LC3 puncta (autophagosomes) in HeLa/GFP-LC3 cells treated with non-targeting control siRNA (NC) or *ATG7* siRNA for 72 h and then mock-infected or infected with SIN or HSV-1ΔBBD (at a multiplicity of infection [MOI] of 10 and 5, respectively; 4.5 h) in the presence or absence of the lysosomal inhibitor bafilomycin A1 (Baf A1, 100 nM) for 1 h prior to fixation. Scale

bars, 20 μm. Arrows denote representative autophagosomes that would be scored as positive in **b** and **c**. The box plot with whiskers from minimum to maximum in **b** represents 100-150 cells analyzed for one of triplicate samples per condition. Bars in **c** represent mean ± s.d. of triplicate samples (100-150 cells analyzed per sample). Similar results were observed in three independent experiments. Both analyses were performed for similar fluorescence microscopy experiments in Figs. 1, 3, and Extended Data Figs. 1, 3, 4, 8, 9, 10, and only bar graphs are shown. **d**, Western blot analyses of indicated proteins in HeLa/GFP-LC3 cells treated with NC or *ATG7* siRNA for 72 h as in **a**-**c**. **e**-**g**, Representative western blot detection (**e**) and quantitation (**f**, **g**) of indicated proteins in lysates (prepared with Triton X-100 lysis buffer) of HeLa cells mock-infected or infected with SIN or HSV-1ΔBBD (MOI = 10 and 5, respectively; 7 h) with the presence or absence of Baf A1 (100 nM) for 2 h (from 5 hours post infection [hpi] to 7 hpi). Bars in **f** and **g** represent mean ± s.d. of LC3-II/LC3-I ratios (**f**) and p62/actin ratios (**g**) of three independent experiments, respectively. **h**, **i**, Representative western blot detection (**h**) and quantitation (**i**) of p62 and actin in lysates (prepared with SDS lysis buffer) of HeLa cells mock-infected or infected with SIN or HSV-1ΔBBD (MOI = 10 and 5, respectively; 7 h). Bars in **i** represent mean ± s.d. of p62/actin ratios of three independent experiments. **j**, Quantitation of GFP-LC3 puncta in HeLa/GFP-LC3 cells treated with NC or *ATG13* siRNA for 72 h and then mock-infected or infected with SIN or HSV-1ΔBBD (MOI = 10 and 5, respectively; 4.5 h). **k**, Western blot analyses of indicated proteins in HeLa/GFP-LC3 cells treated with NC or *ATG13* siRNA for 72 h as in **j**. **l**, Quantitation of GFP-LC3 puncta in HeLa/GFP-LC3 cells mock-infected or infected with SIN or HSV-1ΔBBD (MOI = 10 and 5, respectively; 4.5 h) and treated with PIK-III (5 μM), Baf A1 (100 nM) or DMSO control for 1 h (from 3.5 hpi to 4.5 hpi). Bars in **j** and **l** represent mean ± s.d. of triplicate samples (100-150 cells analyzed per sample). Similar results were observed in three independent experiments. Unpaired two-tailed *t*-tests were used to compare means of Baf A1- versus DMSO-treated cells, those of *ATG13* siRNA- versus NC-treated cells, and those of PIK-III- versus DMSO-treated cells. One-way ANOVA with Dunnett's test for multiple comparisons was used to compare means of SIN or HSV-1ΔBBD infection versus mock infection. For gel source data, see Supplementary Fig. 1.

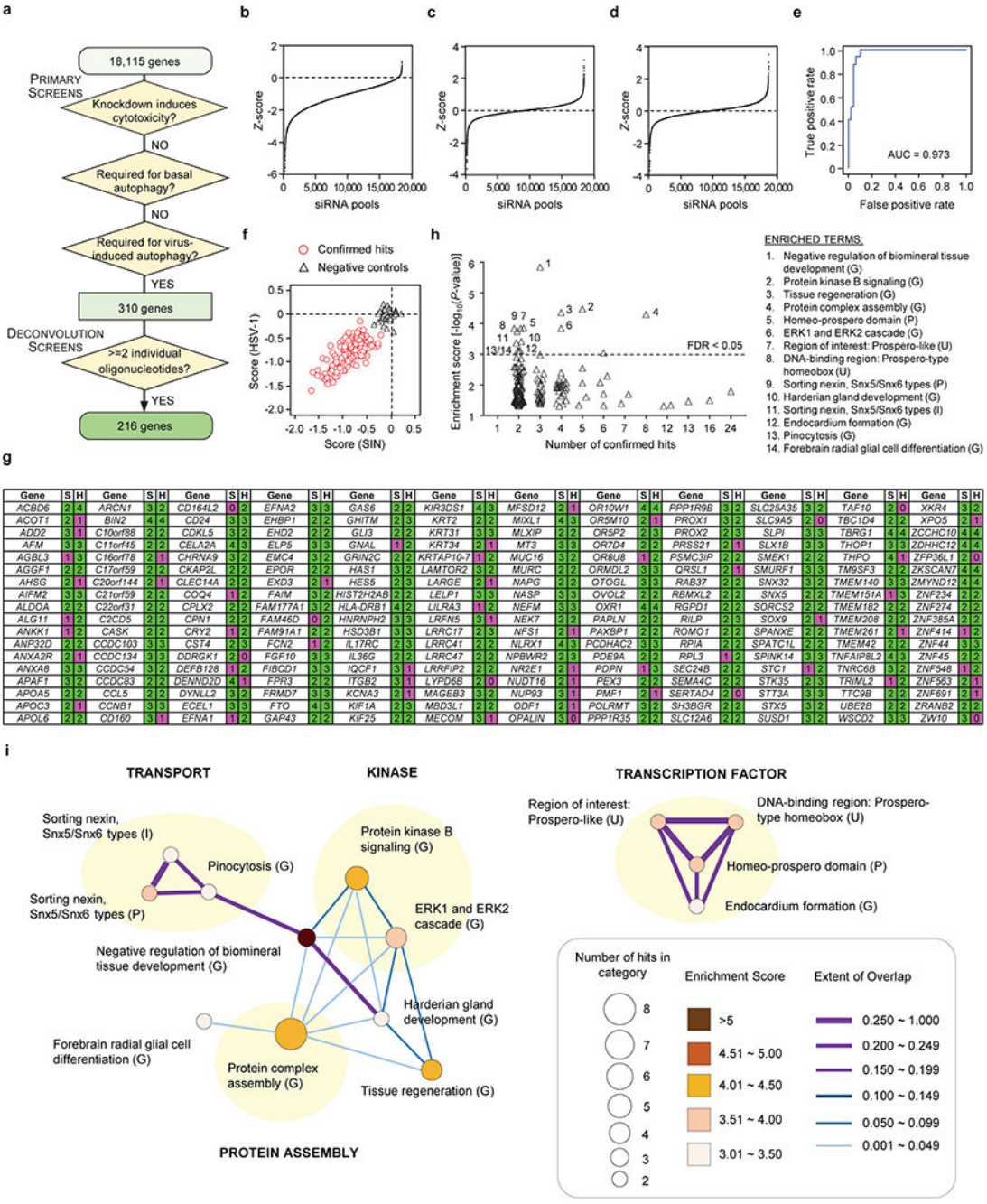

Gene	S	H	Gene	S	H	Gene	S	H	Gene	S	H	Gene	S	H	Gene	S	H	Gene	S	H	Gene	S	H	Gene	S	H	Gene	S	H
ACBD6	2	4	*ARCN1*	3	2	*CD164L2*	0	2	*EFNA2*	3	3	*GAS6*	2	2	*KIR3DS1*	4	3	*MFSD12*	2	1	*OR10W1*	4	4	*PPP1R9B*	3	2	*SLC25A35*	3	2	*TAF10*	2	0	*XKR4*	3	2
ACOT1	2	1	*BIN2*	4	4	*CD24*	3	3	*EHBP1*	2	2	*GHITM*	2	3	*KRT2*	2	2	*MIXL1*	4	3	*OR5M10*	2	1	*PROX1*	3	2	*SLC9A5*	2	0	*TBC1D4*	2	2	*XPO5*	2	1
ADD2	3	1	*C10orf88*	2	2	*CDKL5*	3	2	*EHD2*	2	2	*GLI3*	2	2	*KRT31*	3	3	*MLXIP*	2	2	*OR5P2*	2	3	*PROX2*	2	3	*SLPI*	3	3	*TBRG1*	4	4	*ZCCHC10*	4	4
AFM	3	3	*C11orf45*	2	2	*CELA2A*	4	3	*ELP5*	3	3	*GNAL*	1	2	*KRT34*	2	1	*MT3*	3	3	*OR7D4*	2	2	*PRSS21*	2	1	*SLX1B*	3	3	*THOP1*	3	3	*ZDHHC12*	4	4
AGBL3	1	3	*C16orf78*	2	1	*CHRNA9*	3	2	*EMC4*	3	2	*GRIN2C*	2	2	*KRTAP10-7*	1	2	*MUC16*	3	2	*OR8U8*	1	2	*PSMC3IP*	2	2	*SMEK1*	2	2	*THPO*	4	1	*ZFP36L1*	2	0
AGGF1	2	2	*C17orf59*	2	2	*CKAP2L*	2	2	*EPOR*	2	2	*HAS1*	3	2	*LAMTOR2*	3	2	*MURC*	2	2	*ORMDL2*	3	3	*QRSL1*	2	1	*SMURF1*	3	3	*TM9SF3*	2	2	*ZKSCAN7*	4	4
AHSG	2	1	*C20orf144*	2	1	*CLEC14A*	2	2	*EXD3*	2	1	*HES5*	2	3	*LARGE*	2	1	*NAPG*	2	2	*OTOGL*	3	3	*RAB37*	2	2	*SNX32*	3	2	*TMEM140*	3	3	*ZMYND12*	4	4
AIFM2	3	3	*C21orf59*	2	2	*COQ4*	1	2	*FAIM*	3	2	*HIST2H2AB*	2	2	*LELP1*	3	3	*NASP*	3	3	*OVOL2*	2	2	*RBMXL2*	2	2	*SNX5*	2	2	*TMEM151A*	1	3	*ZNF234*	2	2
ALDOA	2	2	*C22orf31*	2	2	*CPLX2*	2	2	*FAM177A1*	3	2	*HLA-DRB1*	4	2	*LILRA3*	1	2	*NEFM*	3	3	*OXR1*	4	4	*RGPD1*	2	2	*SORCS2*	2	2	*TMEM182*	2	2	*ZNF274*	2	2
ALG11	1	2	*C2CD5*	2	2	*CPN1*	2	2	*FAM46D*	0	2	*HNRNPH2*	3	3	*LRFN5*	3	1	*NEK7*	2	2	*PAPLN*	2	2	*RILP*	2	3	*SOX9*	2	1	*TMEM208*	2	2	*ZNF385A*	2	2
ANKK1	1	2	*CASK*	2	2	*CRY2*	1	2	*FAM91A1*	2	2	*HSD3B1*	3	3	*LRRC17*	2	3	*NFS1*	2	1	*PAXBP1*	2	2	*ROMO1*	2	2	*SPANXE*	2	2	*TMEM261*	2	1	*ZNF414*	1	2
ANP32D	2	2	*CCDC103*	3	3	*CST4*	2	3	*FCN2*	1	2	*IL17RC*	2	3	*LRRC41*	2	2	*NLRX1*	4	3	*PCDHAC2*	3	3	*RPIA*	2	2	*SPATC1L*	2	2	*TMEM42*	2	2	*ZNF44*	3	3
ANXA2R	2	1	*CCDC134*	3	3	*DDRGK1*	2	0	*FGF10*	3	3	*IL36G*	2	2	*LRRC47*	2	2	*NPBWR2*	2	3	*PDE9A*	2	2	*RPL3*	1	2	*SPINK14*	3	3	*TNFAIP8L2*	4	3	*ZNF45*	2	2
ANXA8	3	3	*CCDC54*	3	2	*DEFB128*	1	2	*FIBCD1*	3	3	*IQCF1*	3	1	*LRRFIP2*	2	2	*NR2E1*	2	1	*PDPN*	1	3	*SEC24B*	2	2	*STC1*	1	2	*TNRC6B*	3	2	*ZNF548*	1	2
APAF1	3	2	*CCDC83*	2	2	*DENND2D*	4	1	*FPR3*	2	2	*ITGB2*	3	1	*LYPD6B*	2	0	*NUDT16*	2	1	*PEX3*	2	2	*SEMA4C*	2	2	*STK35*	2	3	*TRIML2*	1	2	*ZNF563*	2	1
APOA5	2	2	*CCL5*	2	2	*DYNLL2*	3	2	*FRMD7*	3	3	*KCNA3*	2	1	*MAGEB3*	3	2	*NUP93*	3	1	*PMF1*	2	1	*SERTAD4*	2	0	*STT3A*	3	3	*TTC9B*	2	2	*ZNF691*	2	1
APOC3	2	1	*CCNB1*	3	3	*ECEL1*	3	3	*FTO*	4	3	*KIF1A*	2	3	*MBD3L1*	2	2	*ODF1*	2	1	*POLRMT*	3	2	*SH3BGR*	2	2	*STX5*	3	2	*UBE2B*	2	2	*ZRANB2*	2	2
APOL6	2	2	*CD160*	3	1	*EFNA1*	1	2	*GAP43*	2	2	*KIF25*	2	2	*MECOM*	3	1	*OPALIN*	3	0	*PPP1R35*	2	2	*SLC12A6*	2	2	*SUSD1*	3	2	*WSCD2*	3	3	*ZW10*	3	0

Extended Data Fig. 2. Schematic summary, statistical analyses and functional enrichment analyses of genome-wide siRNA screens.

a, Flowchart summary of primary and deconvolution siRNA screens in HeLa/GFP-LC3 cells. Three filters were applied in the primary siRNA screens: (1) absence of cytotoxicity of siRNA pools in transfected cells; (2) lack of effect of siRNA pools on numbers of GFP-LC3 puncta in mock-infected cells (basal autophagy); and (3) significant reduction of numbers of GFP-LC3 puncta in cells infected with either SIN or HSV-1ΔBBD (virus-induced autophagy). In the deconvolution siRNA screens, positive hits were defined as those genes

with two or more individual siRNA oligonucleotides from siRNA pools that reproduced the phenotype of the siRNA pools. **b**-**d**, Ranked distribution of median scores for each siRNA pool in primary siRNA screens. Dots shown in graphs denote median scores of GFP-LC3 puncta in mock-infected cells (**b**), SIN-infected cells (**c**) and HSV-1ΔBBD-infected cells (**d**). **e**, A representative receiver operating characteristic (ROC) curve of quality control plates for primary and deconvolution screens. The ROC mean ± s.d. of all the quality control plates was 0.97 ± 0.03, which indicates accuracy and specificity in the identification of cellular factors that regulate numbers of GFP-LC3 puncta. **f**, Scatter plot of median scores of 216 confirmed hits from the deconvolution siRNA screens (open circles) and 40 negative on-plate controls (open triangles). Scores are medians from triplicate assay plates of four individual siRNA oligonucleotides per gene. The 216 confirmed hits and 40 negative on-plate controls fall into two distinct clusters. **g**, Gene list from deconvolution screens for virus-induced autophagy during infection with Sindbis virus (S) and HSV-1ΔBBD (H). Numbers denote number of individual siRNA oligonucleotides that scored positive in each screen. Green, genes with 2 or more positive siRNA oligonucleotides (confirmed hits); magenta, genes with <2 positive siRNA oligonucleotides (non-confirmed hits). **h**, Enrichment analyses of gene sets including molecular function, biological process, cellular component and protein domain categories (terms) from DAVID Bioinformatics Resources. There were 174 terms (open triangles) that contain at least two confirmed hits and have hypergeometric test *P*-values less than 0.05; fourteen of these terms exhibited false discovery rate (FDR) adjusted *P*-values less than 0.05. The enrichment score was defined as $-\log_{10}$ (hypergeometric test *P*-value). **i**, Fourteen highly enriched terms plotted as a network graph. Each node represents a gene set from a variety of categories (indicated in brackets) as follows: G, GOTERM; I, INTERPRO; P, PIR_SUPERFAMILY, U, UP_SEQ_FEATURE. The size of each node corresponds to the number of confirmed siRNA hits and the color intensity is scaled according to the enrichment score. The thickness and color intensity of lines connecting two nodes correspond to the extent of overlapping genes between two gene sets. See Fig. 1a and Supplementary Tables 1 to 5 for further details.

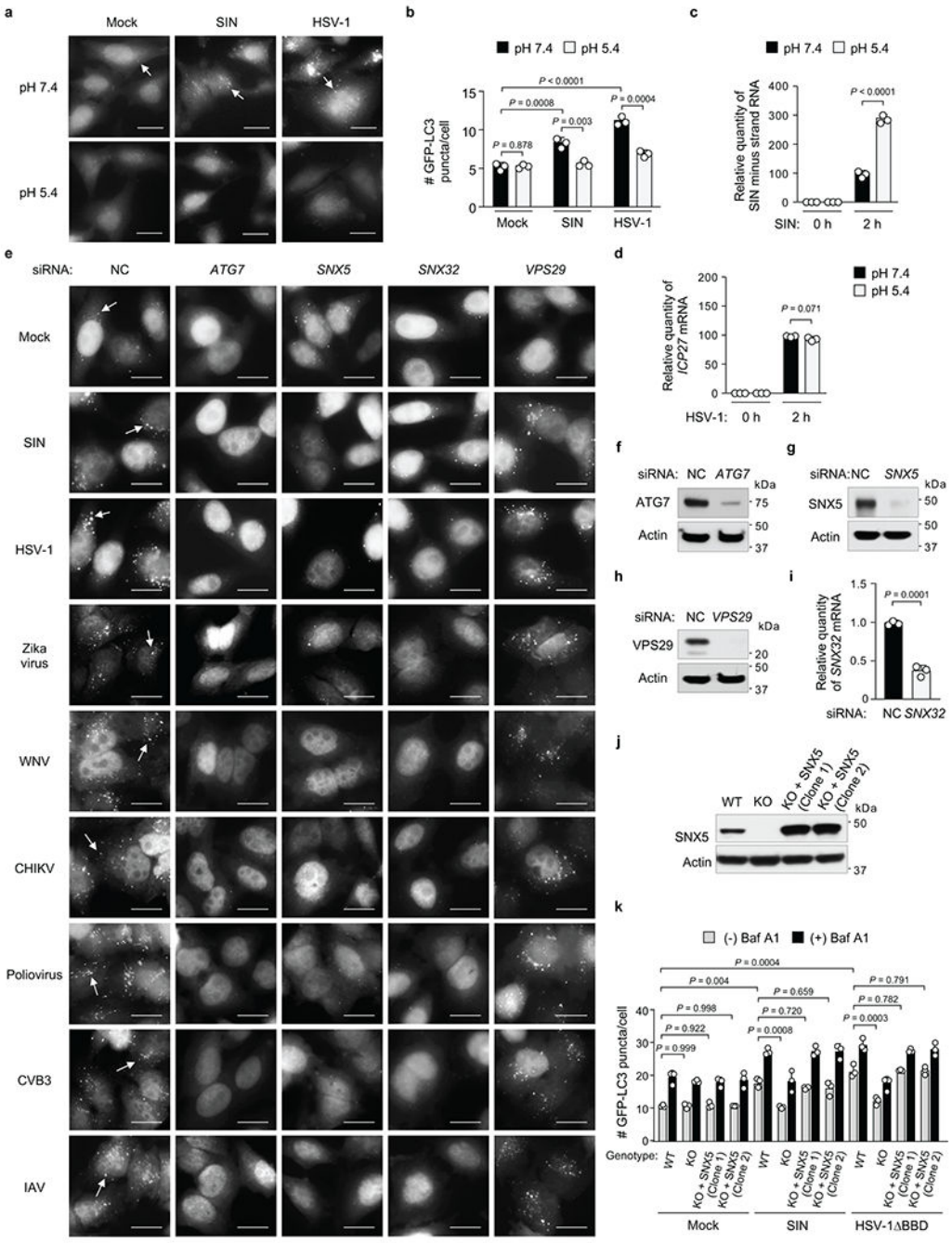

Extended Data Fig. 3. Impaired autophagy induction by acid-mediated bypass of endocytic viral entry, confirmation of indicated gene knockdown in HeLa cells, and requirement for SNX5 in autophagy induced by diverse viruses.

a, **b**, Representative fluorescent micrographs (**a**) and quantitation (**b**) of GFP-LC3 puncta in HeLa/GFP-LC3 cells that were either mock-infected or infected with SIN or HSV-1ΔBBD (MOI = 50 and 25, respectively; 4.5 h) in the presence (pH 5.4) or absence (pH 7.4) of an acidic pulse (that induces viral entry at the plasma membrane) after viral attachment. Arrows in **a** denote representative GFP-LC3 puncta that would be scored as positive in **b**. Scale bars, 20 μm. Bars in **b** represent mean ± s.d. of triplicate samples (100-150 cells analyzed per

sample). **c**, **d**, Viral entry efficiency in HeLa/GFP-LC3 cells treated similarly as in **a** and **b**. Bars in **c** and **d** represent mean ± s.d. of SIN minus-strand RNA levels (**c**) and HSV-1 immediate early gene *ICP27* mRNA levels (**d**) of triplicate samples at indicated time points, respectively. **e**, Representative fluorescent micrographs of GFP-LC3 puncta in HeLa/GFP-LC3 cells that were treated with indicated siRNAs (72 h) and then either mock-infected or infected with indicated virus for 4.5 h (MOI = 10 for SIN, Zika virus, WNV, CHIKV and IAV; MOI = 5 for HSV-1ΔBBD; and MOI = 20 for poliovirus and CVB3). Scale bars, 20 μm. Arrows in **e** denote representative GFP-LC3 puncta that would be scored as positive in Fig. 1b. **f**-**i**, Confirmation of gene knockdown in indicated siRNA-treated HeLa/GFP-LC3 cells (72 h) by western blot analyses of indicated proteins (**f**-**h**) or quantitative real-time PCR of *SNX32* (**i**) for the experiment shown in Fig. 1b. Bars in **i** represent mean ± s.d. of triplicate samples. **j**, Western blot detection of SNX5 and actin in wild-type HeLa/GFP-LC3 cells (WT), HeLa $SNX5^{KO}$/GFP-LC3 cells (KO), and two clones of reconstituted HeLa $SNX5^{KO}$/GFP-LC3/SNX5 cells used in the experiment shown in **k**. In **b**, one-way ANOVA with Dunnett's test for multiple comparisons was used to compare means of SIN or HSV-1ΔBBD infection versus mock infection. In **b**-**d**, unpaired two-tailed *t*-tests were used to compare means of pH7.4 versus pH5.4 conditions. For **e-h, j**, similar results were observed in three independent experiments. In **i**, an unpaired two-tailed *t*-test was used to compare means of NC versus *SNX32* knockdown. **k**, GFP-LC3 puncta in reconstituted HeLa $SNX5^{KO}$/GFP-LC3 cells mock-infected or infected with SIN or HSV-1ΔBBD (MOI = 10 and 5, respectively; 4.5 h). Bars represent mean ± s.d. of three independent replicates (100-150 cells per sample). *P*-values, one-way ANOVA with Dunnett's test for multiple comparisons. For gel source data, see Supplementary Fig. 1.

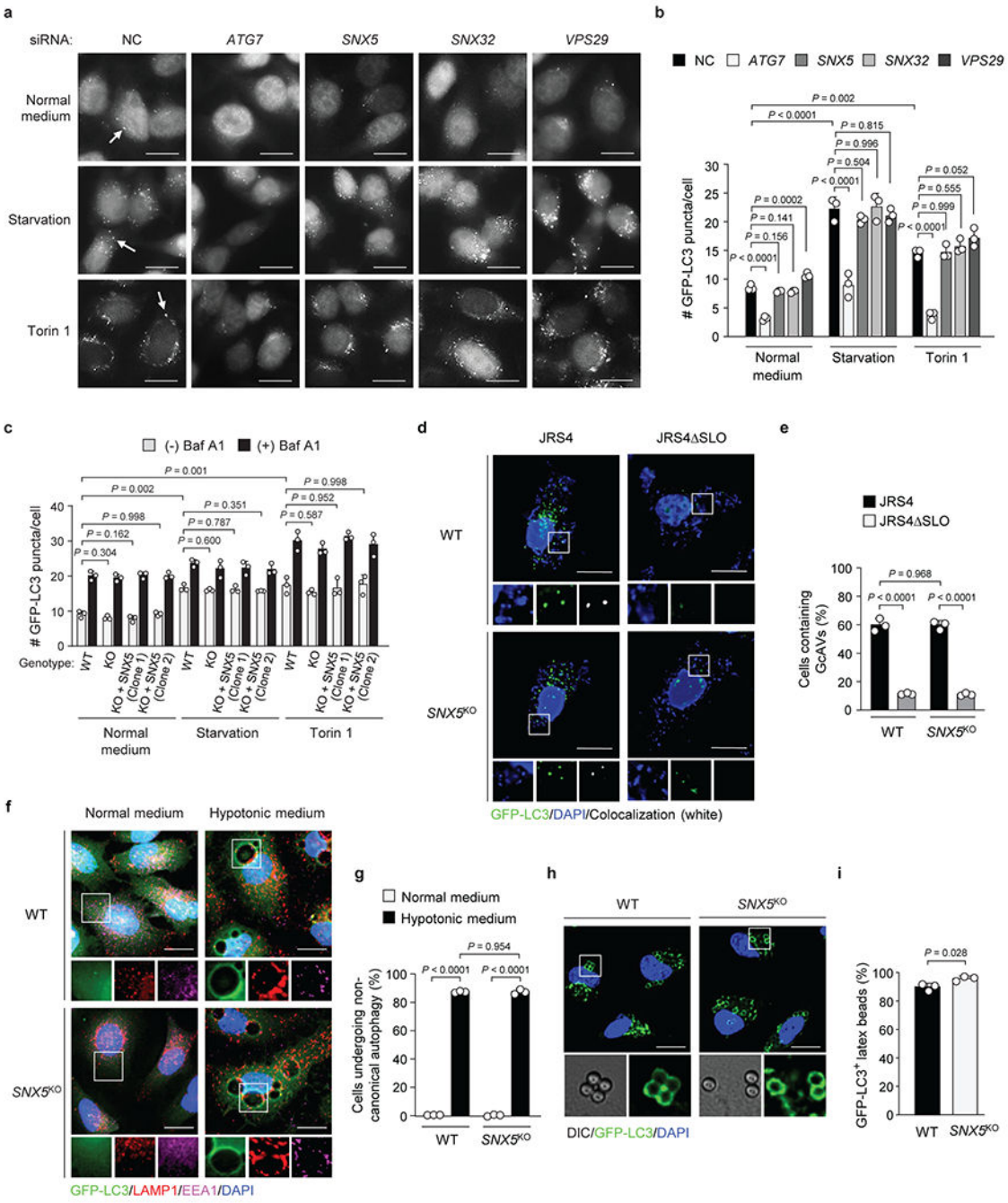

Extended Data Fig. 4. SNX5 is dispensable for general autophagy or non-canonical forms of autophagy that require LC3 recruitment to endolysosomal or phagosomal compartments in HeLa cells.

a, **b**, Representative fluorescent micrographs (**a**) and quantitation (**b**) of GFP-LC3 puncta in HeLa/GFP-LC3 cells that were treated with indicated siRNA (72 h) and then cultured in normal medium (1 h), starvation medium (EBSS; 1 h), or normal medium containing torin 1 (250 nM; 1 h). Scale bars, 20 μm. Arrows denote representative autophagosomes that would be scored as positive in **b**. **c**, Quantitation of GFP-LC3 puncta in wild-type HeLa/GFP-LC3 cells (WT), HeLa *SNX5*^{KO}/GFP-LC3 cells (KO), and two clones of reconstituted HeLa

SNX5^{KO}/GFP-LC3/SNX5 cells that were cultured in normal medium (1 h), starvation medium (EBSS; 1 h), or normal medium containing torin 1 (250 nM; 1 h). **d**, **e**, Representative fluorescent micrographs (**d**) and quantitation (**e**) of wild-type HeLa/GFP-LC3 cells and HeLa *SNX5*^{KO}/GFP-LC3 cells bearing Group A *Streptococcus*-containing autophagosome-like vacuoles (GcAVs) at 2 h post bacterial infection (MOI = 100) with Group A *Streptococcus* strain JRS4 and the isogenic mutant JRS4ΔSLO (which does not induce formation of GcAVs due to defective bacterial escape from endosomes). Cellular and bacterial DNA was stained with DAPI. Boxed areas are magnified by four-fold to show micrographs of indicated channels and representative GcAVs (white puncta). Scale bars, 20 μm. **f**, **g**, Representative fluorescent micrographs (**f**) and quantitation (**g**) of wild-type HeLa/GFP-LC3 cells and HeLa *SNX5*^{KO}/GFP-LC3 cells undergoing non-canonical autophagy after being cultured in either normal medium or hypotonic medium for 1 h. Boxed areas are magnified by two-fold to show micrographs of individual channels. Scale bars, 20 μm. **h**, **i**, Representative differential interference contrast (DIC) microscopy and fluorescence microscopy micrographs (**h**) and quantitation (**i**) of monensin-driven LC3-associated phagocytosis (LAP) of latex beads in wild-type HeLa/GFP-LC3 cells and HeLa *SNX5*^{KO}/GFP-LC3 cells that were treated with monensin (100M) and polybead microspheres (3 μm in diameter) for 1 h. Boxed areas are magnified by nine-fold to show micrographs of DIC channel and GFP channel. Scale bars, 20 μm. In **b**, **c**, **e**, **g** and **i**, bars represent mean ± s.d. of triplicate samples (100-150 cells analyzed per sample). *P*-values were determined with one-way ANOVA with Dunnett's test for multiple comparisons (**b** and **c**) or unpaired two-tailed *t*-test (**e**, **g** and **i**). For **a**, **d**, **f**, and **h**, similar results were observed in three independent experiments.

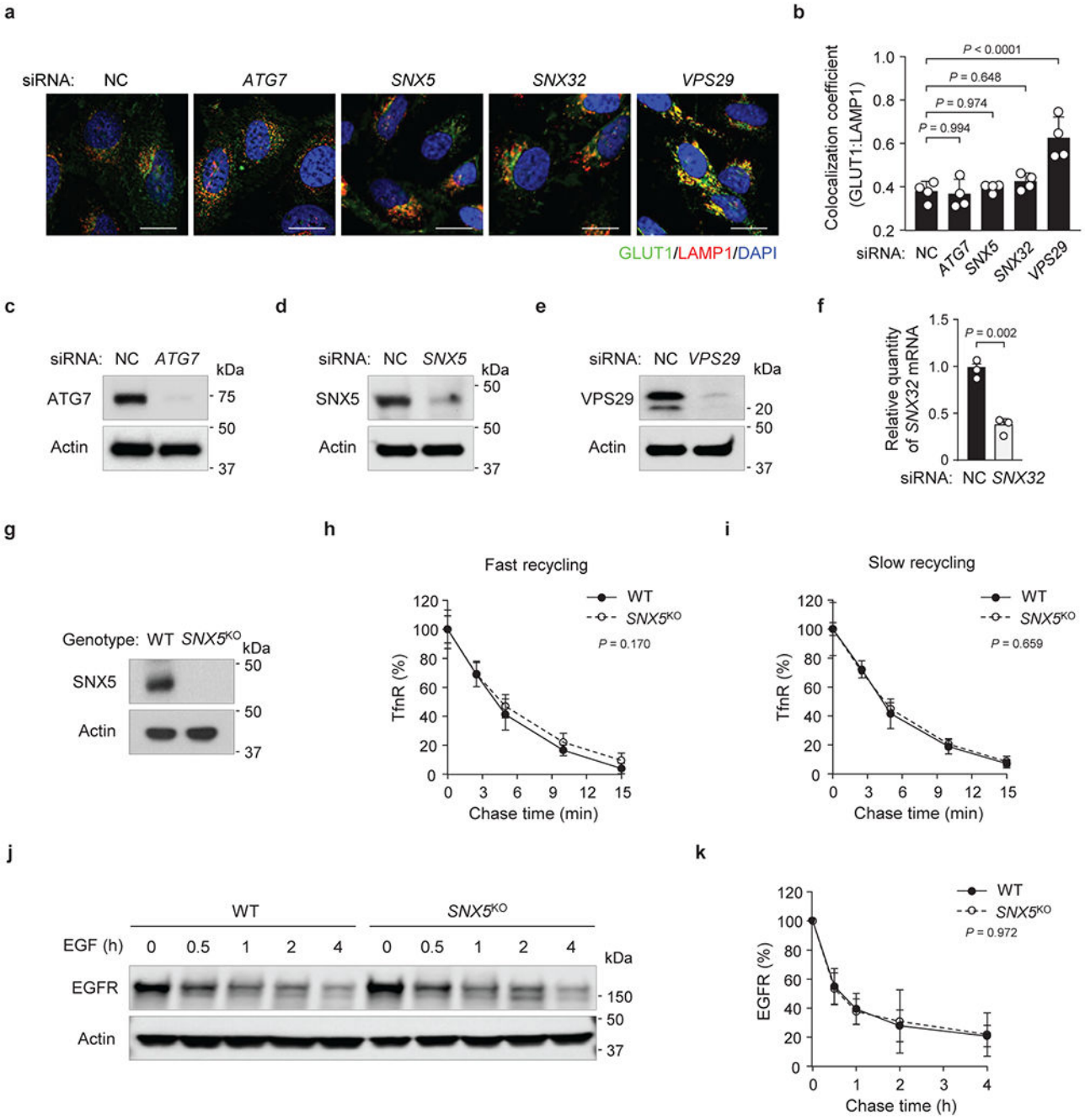

Extended Data Fig. 5. SNX5 is not required for retromer function and endolysosomal function in HeLa cells.

a, **b**, Representative fluorescent micrographs (**a**) and quantitation (**b**) of GLUT1 colocalized with the lysosomal marker LAMP1 in HeLa cells treated with indicated siRNA (72 h). Colocalized GLUT1 and LAMP1 puncta (yellow) represent lysosomal localization of mis-sorted GLUT1 which increases when retromer function is defective. Scale bars, 20 μm. Bars in **b** represent mean ± s.d. of Manders' overlap coefficient of GLUT1 and LAMP1 of four replicates. **c-f**, Confirmation of gene knockdown in indicated siRNA-treated HeLa cells (72

h) for experiments shown in **a** and **b** by western blot analyses of indicated proteins (**c**-**e**) or quantitative real-time PCR of *SNX32* (**f**). Bars in **f** represent mean ± s.d. of triplicate samples. Similar results were observed in three independent experiments. **g**, Western blot detection of SNX5 and actin in HeLa $SNX5^{KO}$ cells and parental wild-type (WT) HeLa cells. **h**, **i**, Quantitation of remaining protein levels of internalized plasma membrane-anchored transferrin receptor (TfnR) in WT and $SNX5^{KO}$ HeLa cells during fast (**h**) and slow (**i**) endocytic recycling processes. **j**, **k**, Representative western blot analysis (**j**) and densitometry analysis (**k**) of epidermal growth factor receptor (EGFR) and actin in WT and $SNX5^{KO}$ HeLa cells at indicated chase time after treating with EGF (100 ng/mL). Symbols in **h**, **i** and **k** represent mean ± s.d. of three independent experiments. *P*-values were determined with one-way ANOVA with Dunnett's test for multiple comparisons (**b**), unpaired two-tailed *t*-test (**f**) or repeated measures ANOVA (**h**, **i** and **k**). For **a**, **c**-**e**, **g**, and **j**, similar results were observed in three independent experiments. For gel source data, see Supplementary Fig. 1.

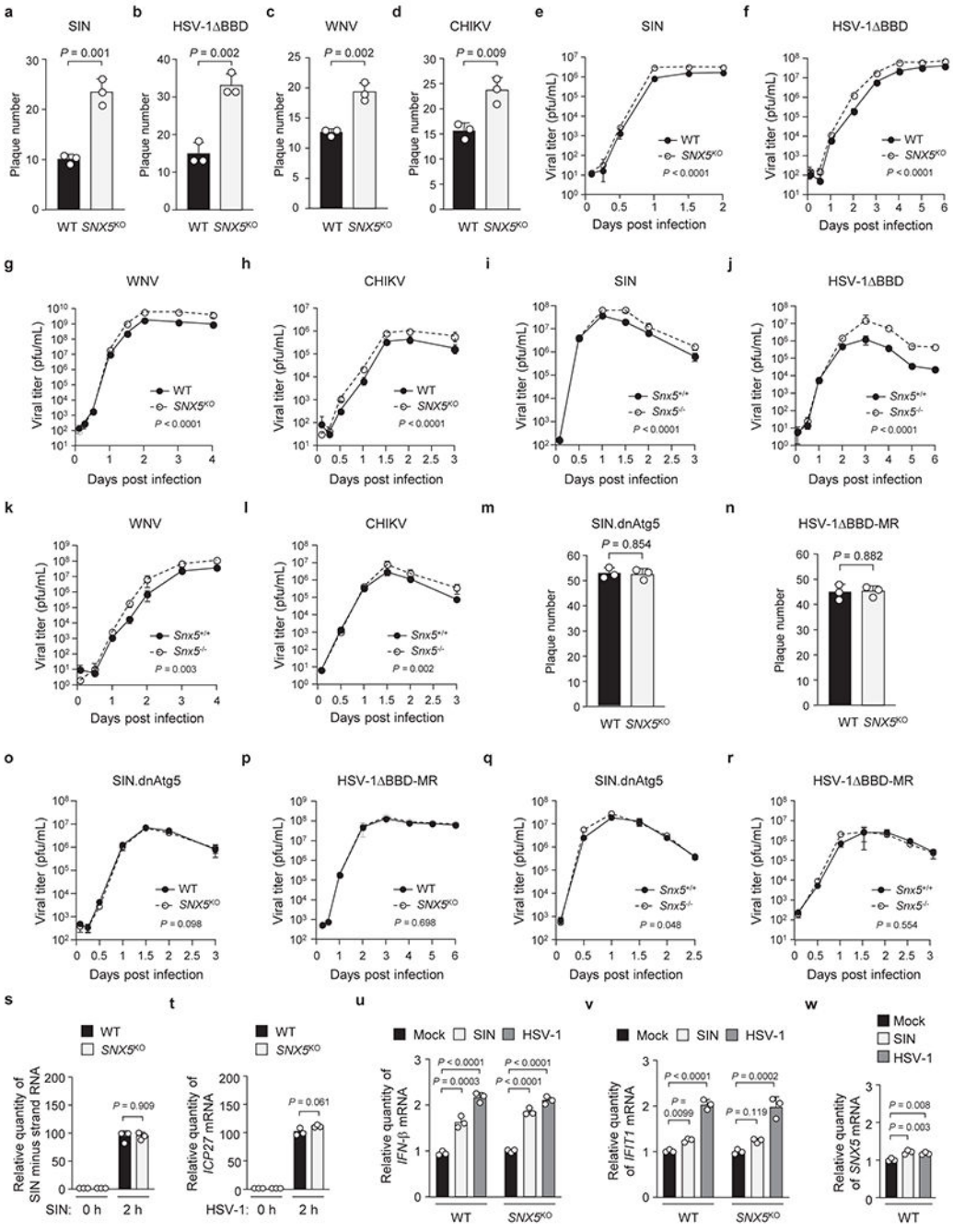

Extended Data Fig. 6. SNX5 restricts viral infection in HeLa cells and primary mouse embryonic fibroblasts (MEFs) via an autophagy-dependent mechanism.

a-**d**, Viral infectivity assay in WT and *SNX5*^{KO} HeLa cells infected with indicated virus. **e**-**h**, Viral multi-step growth curves (MOI = 0.01) of WT and *SNX5*^{KO} HeLa cells infected with indicated virus. **i**-**l**, Viral multi-step growth curves (MOI = 0.01) of *Snx5*$^{+/+}$ and *Snx5*$^{-/-}$ primary MEFs infected with indicated virus. **m**, **n**, Viral infectivity assay in WT and *SNX5*^{KO} HeLa cells infected with autophagy-suppressive viral strains, SIN.dnAtg5 and HSV-1ΔBBD-MR. **o**-**r**, Viral multi-step growth curves (MOI = 0.01) of WT and *SNX5*^{KO}

HeLa cells (**o**, **p**) and *Snx5*$^{+/+}$ and *Snx5*$^{-/-}$ primary MEFs (**q**, **r**) infected with SIN.dnAtg5 (**o**, **q**) and HSV-1ΔBBD-MR (**p**, **r**). In **a**-**d**, **m** and **n**, bars represent mean ± s.d. of the number of viral plaques formed in cell monolayers of three replicates. In **e**-**l** and **o**-**r**, symbols represent mean ± s.d. of viral titer of three replicates. **s**, **t**, Viral entry efficiency in WT and *SNX5*^{KO} HeLa cells that were infected with SIN (MOI = 50) or HSV-1ΔBBD (MOI = 25). Bars in **s** and **t** represent mean ± s.d. of SIN minus-strand RNA levels (**s**) and HSV-1 immediate early gene *ICP27* mRNA levels (**t**) of triplicate samples at indicated time point, respectively. **u**, **v**, Quantitative real-time PCR analyses of relative mRNA levels of interferon beta (*IFN*-β; **u**) and the interferon-stimulated gene (ISG) interferon induced protein with tetratricopeptide repeats 1 (*IFIT1*; **v**) in WT and *SNX5*^{KO} HeLa cells that were mock-infected or infected with SIN or HSV-1ΔBBD (MOI = 10 and 5, respectively; 4.5 h). **w**, Quantitative real-time PCR analyses of relative mRNA levels of *SNX5* in WT HeLa cells that were infected similarly as in **u** and **v**. In **u**-**w**, bars represent mean ± s.d. of three replicates. *P*-values were determined with unpaired two-tailed *t*-test (**a**-**d**, **m**, **n**, **s** and **t**), repeated measures ANOVA (**e**-**l** and **o**-**r**) or one-way ANOVA with Dunnett's test for multiple comparisons (**u**-**w**). Similar results were observed in three independent experiments.

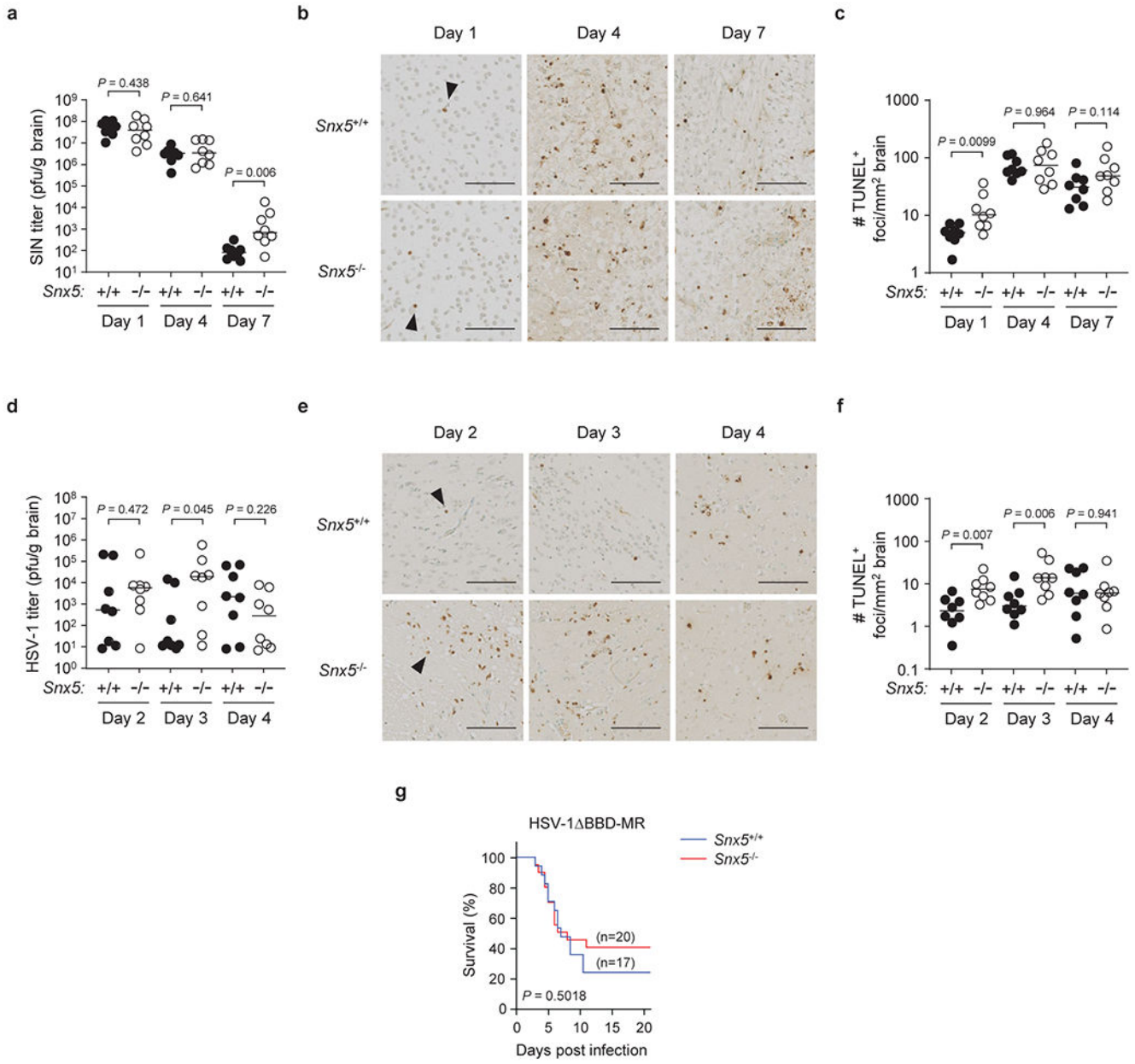

Extended Data Fig. 7. CNS viral titers, neuronal cell death and animal survival of virally-infected *Snx5*$^{+/+}$ and *Snx5*$^{-/-}$ littermate mice.

a-**c**, CNS viral titers (**a**) and neuronal cell death (**b**, **c**) in seven-day-old *Snx5*$^{+/+}$ (n = 8) and *Snx5*$^{-/-}$ (n = 8) littermate mice at indicated time point after infection via intracerebral (i.c.) inoculation with SIN strain dsTE12Q (1,000 pfu/mouse). **d**-**f**, CNS viral titers (**d**) and neuronal cell death (**e**, **f**) in eight- to ten-week-old *Snx5*$^{+/+}$ (n = 8) and *Snx5*$^{-/-}$ (n = 8) littermate mice at indicated time point after infection via i.c. inoculation with HSV-1ΔBBD (50,000 pfu/mouse). In **b** and **e**, shown are representative micrographs of TUNEL staining of mouse brain sections from cerebral cortex (**b**) or basal ganglia (**e**) at indicated time point. Scale bars, 100 μm. Arrowheads denote representative TUNEL-positive foci that would be scored as positive in **c** and **f**. In **a**, **c**, **d** and **f**, each data point represents an individual mouse

and black horizontal lines represent median values. **g**, Kaplan-Meier survival curve of eight- to ten-week-old *Snx5*$^{+/+}$ and *Snx5*$^{-/-}$ littermate mice infected i.c. with the autophagy-suppressive strain HSV-1ΔBBD-MR (500 pfu/mouse). Results represent combined survival data for three independent infection experiments. Similar results were observed in each independent infection. *P*-values were determined with unpaired two-tailed *t*-test (**a**, **c**, **d** and **f**) or two-sided log-rank test (**g**).

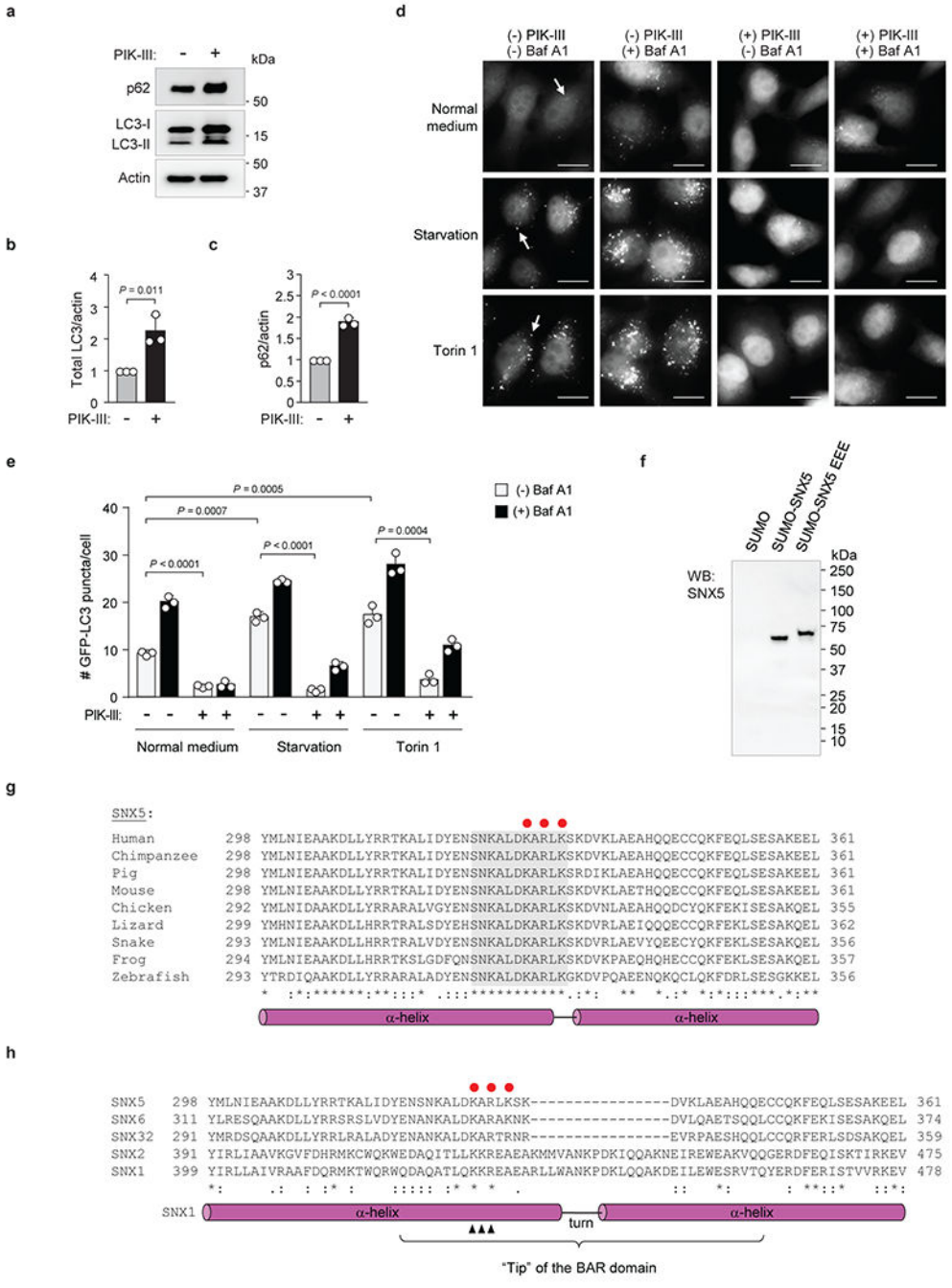

Extended Data Fig. 8. Autophagy inhibition by PIK-III in baseline conditions, starvation and mTOR inhibition; western blot analysis of bacterially-purified SNX5 proteins; and bioinformatic analyses of SNX5 amino-acid sequences (related to Fig. 2).

a-c, Representative western blots (**a**) and densitometry analyses (**b**, **c**) of indicated proteins in WT HeLa cells cultured in normal media in the presence or absence of PIK-III (5 μM) for 1 h. Bars in **b** and **c** represent mean ± s.d. of total LC3/actin ratios (**b**) and p62/actin ratios (**c**) of three replicates. **d**, **e**, Representative fluorescent micrographs (**d**) and quantitation (**e**) of GFP-LC3 puncta in HeLa/GFP-LC3 cells that were cultured in normal medium (1 h), starvation medium (EBSS; 1 h), or normal medium containing torin 1 (250 nM; 1 h) in the presence or absence of PIK-III (5 μM; 1 h) and Baf A1 (100 nM; 1h). Scale bars, 20 μm. Arrows denote representative autophagosomes that would be scored as positive in **e**. Bars in **e** represent mean ± s.d. of three replicates (100-150 cells analyzed per sample). In **b**, **c** and **e**, unpaired two-tailed *t*-test was used to compare means of PIK-III- versus DMSO-treated cells. In **e**, one-way ANOVA with Dunnett's test for multiple comparisons was used to compare means of starvation or torin 1 treatment versus normal condition. **f**, Western blot analysis of His-tagged SUMO, SUMO-SNX5 or SUMO-SNX5 EEE that were used in the experiments shown in Fig. 2c–i. For gel source data, see Supplementary Fig. 1. For **a**, **d**, and **f**, similar results were observed in three independent experiments. **g**, Amino acid sequence alignment of human SNX5 amino acids 298-361 (within the BAR domain) with the homologous regions of Snx5 proteins from eight other vertebrate animals using Cluster Omega (https://www.ebi.ac.uk/Tools/msa/clustalo/). Grey box highlights a highly conserved region across nine vertebrate SNX5 homologs. **h**, Amino acid sequence alignment of human retromer-related sorting nexins. Black arrowheads denote three positively charged residues (K429, K430 and R431) in human SNX1 for which triple mutations to glutamic acid residues (SNX1 EEE) lead to the inability of SNX1 to associate to membranes and induce membrane remodeling[33]. In **g** and **h**, red dots indicate the residues of a positively charged stretch (K328, R330 and K332) in human SNX5 that corresponds to amino acids K429, K430, and R431 in SNX1. The three residues in SNX5 (K328, R330 and K332) were substituted with glutamic acid residues to generate the SNX5 EEE mutant used in this study. Hyphens (-) denote gaps in the indicated sequence identified by sequence alignment. Asterisks (*) indicate positions with a fully conserved residue; colons (:) indicate conserved positions between groups of strongly similar properties (scoring > 0.5 in the Gonnet PAM 250 matrix); periods (.) indicate conserved positions between groups of weakly similar properties (scoring equal to or < 0.5 in the Gonnet PAM 250 matrix). Magenta cylinders represent predicted discontinued alpha helixes using the University College London (UCL) PSIPRED Protein Sequence Analysis Workbench (http://bioinf.cs.ucl.ac.uk/psipred/). Solid line indicates a turn conformation in the tip region of the SNX1 and SNX5 BAR domains[38].

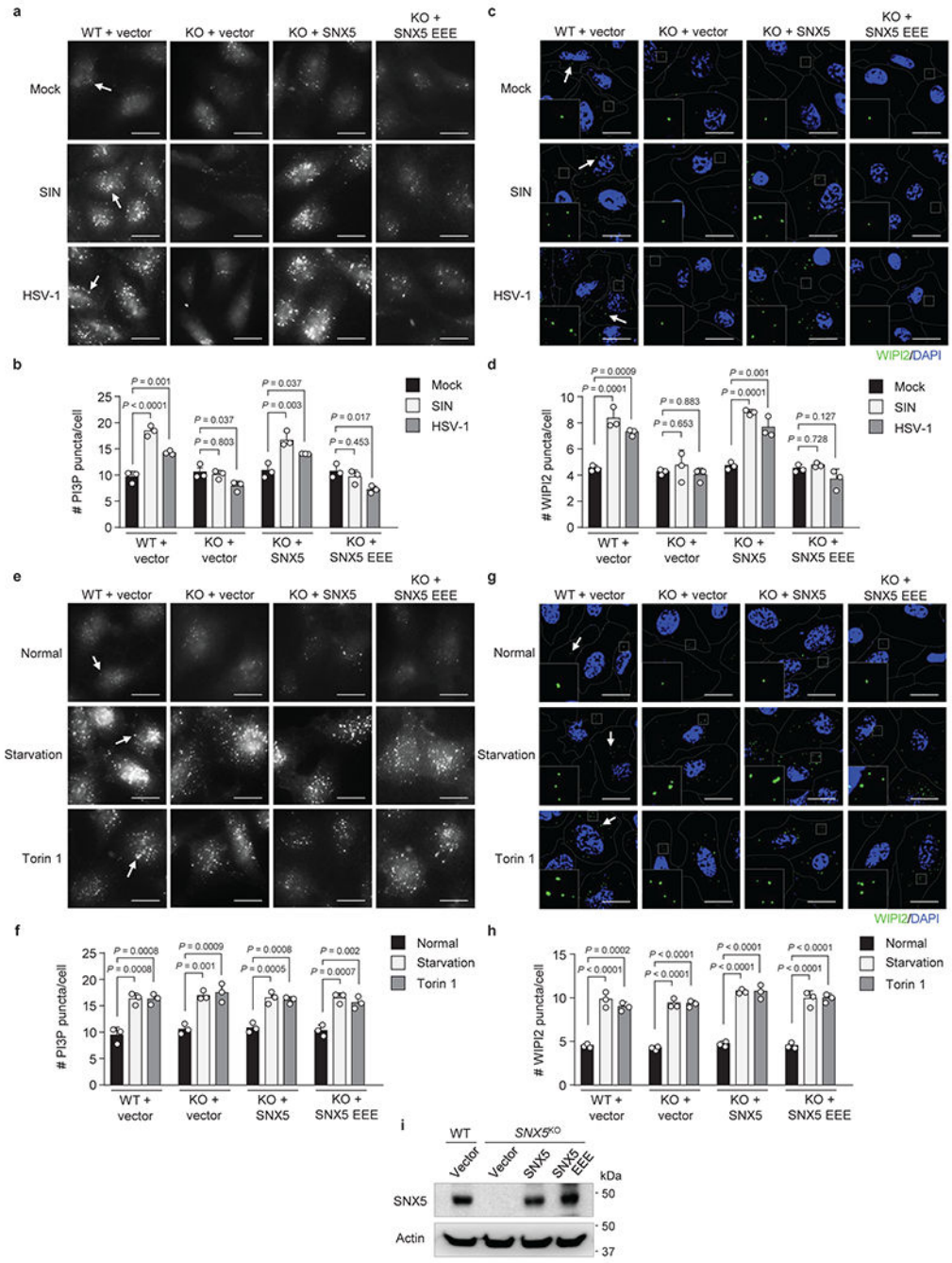

Extended Data Fig. 9. SNX5 is required for formation of PI3P probe puncta and WIPI2 puncta during viral infection, but not in baseline conditions, or upon autophagy induction by starvation or mTOR inhibition.

a-**d**, Representative fluorescent micrographs (**a**, **c**) and quantitation (**b**, **d**) of PI3P probe staining (**a**, **b**) or WIPI2 immunostaining (**c**, **d**) in indicated HeLa cells that were either mock-infected or infected with SIN or HSV-1ΔBBD (MOI = 10 and 5, respectively; 4 h). **e**-**h**, Representative fluorescent micrographs (**e**, **g**) and quantitation (**f**, **h**) of PI3P probe staining (**e**, **f**) or WIPI2 immunostaining (**g**, **h**) in indicated HeLa cells cultured in normal medium (1 h), starvation medium (EBSS; 1 h), or normal medium containing torin 1 (250

nM; 1 h). Scale bars, 20 μm. In **a**, **c**, **e** and **g**, arrows denote representative PI3P probe puncta or WIPI2 puncta that would be scored as positive in **b**, **d**, **f** and **h**. In **c** and **g**, representative cells are outlined by dashed white lines and boxed areas are magnified by sixteen-fold in the insets. In **b**, **d**, **f** and **h**, bars represent mean ± s.d. of three replicates (100-150 cells analyzed per sample). In **b**, **d**, **f** and **h**, *P*-values were determined by one-way ANOVA with Dunnett's test for multiple comparisons. **i**, Western blot analyses of SNX5 and actin in parental wild-type HeLa cells (WT) and HeLa *SNX5*^{KO} cells (KO) reconstituted with either empty vector (WT + vector and KO + vector), wild-type SNX5 (KO + SNX5) or SNX5 EEE mutant (KO + SNX5 EEE). For **a**, **c**, **e**, **g**, and **i**, similar results were observed in three independent experiments. For gel source data, see Supplementary Fig. 1.

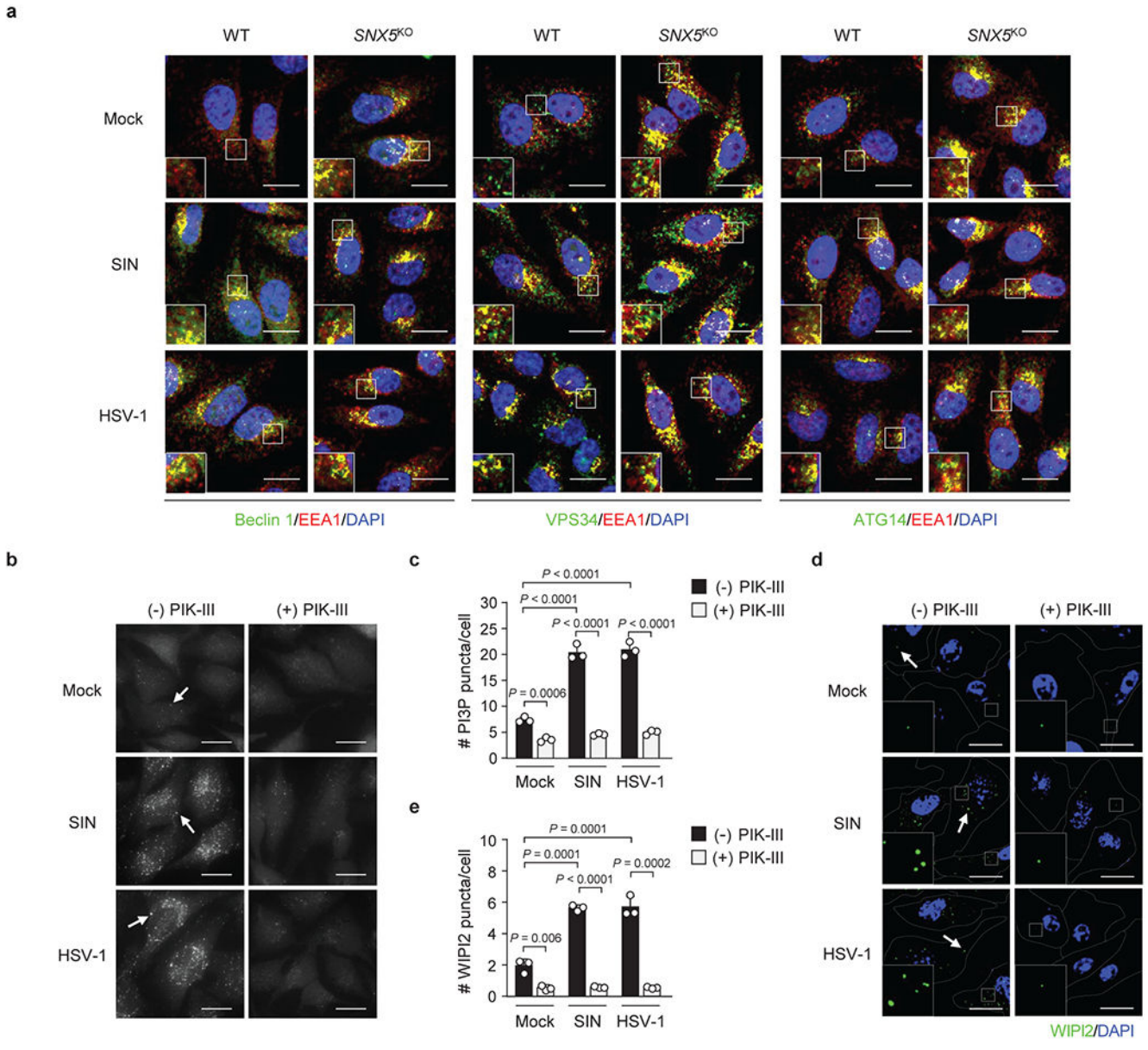

Extended Data Fig. 10. SNX5 is not required for virus-induced endosomal localization of PI3KC3-C1 complexes, and PI3KC3 is required for virus-induced formation of PI3P probe puncta and WIPI2 puncta in HeLa cells.

a, Representative fluorescent micrographs of indicated immunostaining in parental wild-type and *SNX5*^{KO} HeLa cells that were either mock-infected or infected with SIN and HSV-1ΔBBD (MOI = 10 and 5, respectively; 2 h). Scale bars, 20 μm. Boxed areas are magnified by four-fold in the insets. **b**-**e**, Representative fluorescent micrographs (**b** and **d**) and quantitation (**c** and **e**) of PI3P probe staining (**b**, **c**) or WIPI2 immunostaining (**d**, **e**) in HeLa cells that were either mock-infected or infected with SIN or HSV-1ΔBBD (MOI = 10 and 5, respectively; 4 h) and treated for 1 h with PIK-III (5 μM) or DMSO control prior to fixation (from 3 hpi to 4 hpi). Scale bars, 20 μm. Arrows in **b** and **d** denote representative PI3P probe puncta and WIPI2 puncta that would be scored as positive in **c** and **e**, respectively. In **d**, representative cells are outlined by dashed white lines and boxed areas are magnified by sixteen-fold in the insets. Bars in **c** and **e** represent mean ± s.d. of three replicates (100-150 cells analyzed per sample). In **c** and **e**, unpaired two-tailed *t*-test was used to compare means of PIK-III- versus DMSO-treated cells, and one-way ANOVA with Dunnett's test for multiple comparisons was used to compare means of SIN or HSV-1ΔBBD infection versus mock infection. For **a**, **b**, and **d**, similar results were observed in three independent experiments.

Supplementary Material

Refer to Web version on PubMed Central for supplementary material.

Acknowledgments:

This work was supported by Cancer Prevention Research Institute of Texas (CPRIT) grants RP120718 (B.L.) and RP180805 (Y.X.), NIH U19 AI109725 (B.L., R.X.), NIH U19 AI142784 (B.L., R.X.), NIH R01 DK097485 (R.X.), NIH R35 GM130289 (X.Z.), NIH R01 GM115473 (Y.X.), NIH R01 CA172211 (G.X.), the Welch Foundation grant I-1702 (X.Z.), the Rita Allen Foundation (J.W.S.) the Biotechnology and Biological Sciences Research Council grant BB/K019155/1 (N.T.K.), and National Health and Medical Research Council Australia (NHMRC) APP1163862 (P.A.G.). We thank Herbert W. Virgin, Rhea M. Sumpter Jr., Anthony Orvedahl, Milton Packer, David A. Leib, Jennifer Lippincott-Schwartz, Sharon Tooze, Sarah Cherry, Kate Luby-Phelps, Lisa N. Kinch, Chad A. Brautigam, Diana Tomchick, Michael Roth, Michael Shiloh and John Neff for helpful discussions; Melissa Johnson, Hanspeter Niederstrasser and Bruce Posner for assistance with siGENOME siRNA library; Luequn Huang for assistance with high-throughput siRNA screens and data analysis; Yohei Ohashi and Michael Wilson for the design of the PX domain probe and Maria Manifava for assistance in PI3P staining; Abhijit Bugde and the UT Southwestern Medical Center (UTSW) Live Cell Imaging Facility for assistance with fluorescence microscopy; Zhe Chen and Yang Li from the Structural Biology Laboratory at UTSW for assistance with cryo-EM studies (supported in part by CPRIT grant RP170644); Michael S. Diamond, Michael Gale Jr., Adolfo Garcia-Sastre, Deborah J. Lenschow, Karla Kirkegaard, Marco Vignuzzi, Sharon Tooze, Diane E. Griffin, Richard J. Kuhn, Ichiro Nakagawa, Ilya Bezprozvanny, Matthew B. Frieman, Charles M. Rice and Hongwei Wang for providing critical reagents; Lori Nguyen for assistance with animal experiments; and Haley Smith and Heather Kang for assistance with manuscript preparation.

References:

1. Levine B, Mizushima N & Virgin HW Autophagy in immunity and inflammation. Nature 469, 323–335 (2011). [PubMed: 21248839]
2. Dong X & Levine B Autophagy and viruses: adversaries or allies? J Innate Immun 5, 480–493 (2013). [PubMed: 23391695]
3. Merino-Trigo A et al. Sorting nexin 5 is localized to a subdomain of the early endosomes and is recruited to the plasma membrane following EGF stimulation. J Cell Sci 117, 6413–6424 (2004). [PubMed: 15561769]

4. Wassmer T et al. A loss-of-function screen reveals SNX5 and SNX6 as potential components of the mammalian retromer. J Cell Sci 120, 45–54 (2007). [PubMed: 17148574]
5. Orvedahl A et al. HSV-1 ICP34.5 confers neurovirulence by targeting the Beclin 1 autophagy protein. Cell Host Microbe 1, 23–35 (2007). [PubMed: 18005679]
6. Orvedahl A et al. Autophagy protects against Sindbis virus infection of the central nervous system. Cell Host Microbe 7, 115–127 (2010). [PubMed: 20159618]
7. Sumpter R Jr. et al. Fanconi anemia proteins function in mitophagy and immunity. Cell 165, 867–881 (2016). [PubMed: 27133164]
8. Lei Y et al. The mitochondrial proteins NLRX1 and TUFM form a complex that regulates type I interferon and autophagy. Immunity 36, 933–946 (2012). [PubMed: 22749352]
9. Mercer J, Schelhaas M & Helenius A Virus entry by endocytosis. Annu Rev Biochem 79, 803–833 (2010). [PubMed: 20196649]
10. Mim C & Unger VM Membrane curvature and its generation by BAR proteins. Trends Biochem Sci 37, 526–533 (2012). [PubMed: 23058040]
11. Gallop JL & McMahon HT BAR domains and membrane curvature: bringing your curves to the BAR. Biochem Soc Symp 72, 223–231 (2005).
12. Levine B, Liu R, Dong X & Zhong Q Beclin orthologs: integrative hubs of cell signaling, membrane trafficking, and physiology. Trends Cell Biol 25, 533–544 (2015). [PubMed: 26071895]
13. Liu Y et al. Inflammation-induced, STING-dependent autophagy restricts Zika virus infection in the Drosophila brain. Cell Host Microbe 24, 57–68 (2018). [PubMed: 29934091]
14. Kobayashi S et al. Autophagy inhibits viral genome replication and gene expression stages in West Nile virus infection. Virus Res 191, 83–91 (2014). [PubMed: 25091564]
15. Joubert PE et al. Chikungunya virus-induced autophagy delays caspase-dependent cell death. J Exp Med 209, 1029–1047 (2012). [PubMed: 22508836]
16. Jackson WT et al. Subversion of cellular autophagosomal machinery by RNA viruses. PLoS Biol 3, e156 (2005). [PubMed: 15884975]
17. Alirezaei M, Flynn CT, Wood MR & Whitton JL Pancreatic acinar cell-specific autophagy disruption reduces coxsackievirus replication and pathogenesis in vivo. Cell Host Microbe 11, 298–305 (2012). [PubMed: 22423969]
18. Gannage M et al. Matrix protein 2 of influenza A virus blocks autophagosome fusion with lysosomes. Cell Host Microbe 6, 367–380 (2009). [PubMed: 19837376]
19. Nakagawa I et al. Autophagy defends cells against invading group A Streptococcus. Science 306, 1037–1040 (2004). [PubMed: 15528445]
20. Florey O, Gammoh N, Kim SE, Jiang X & Overholtzer M V-ATPase and osmotic imbalances activate endolysosomal LC3 lipidation. Autophagy 11, 88–99 (2015). [PubMed: 25484071]
21. Fletcher K et al. The WD40 domain of ATG16L1 is required for its non-canonical role in lipidation of LC3 at single membranes. EMBO J 37, e97840 (2018). [PubMed: 29317426]
22. Simonetti B, Danson CM, Heesom KJ & Cullen PJ Sequence-dependent cargo recognition by SNX-BARs mediates retromer-independent transport of CI-MPR. J Cell Biol 216, 3695–3712 (2017). [PubMed: 28935633]
23. Lim JP, Gosavi P, Mintern JD, Ross EM & Gleeson PA Sorting nexin 5 selectively regulates dorsal-ruffle-mediated macropinocytosis in primary macrophages. J Cell Sci 128, 4407–4419 (2015). [PubMed: 26459636]
24. Yordy B, Iijima N, Huttner A, Leib D & Iwasaki A A neuron-specific role for autophagy in antiviral defense against herpes simplex virus. Cell Host Microbe 12, 334–345 (2012). [PubMed: 22980330]
25. Shoji-Kawata S et al. Identification of a candidate therapeutic autophagy-inducing peptide. Nature 494, 201–206 (2013). [PubMed: 23364696]
26. Fan W, Nassiri A & Zhong Q Autophagosome targeting and membrane curvature sensing by Barkor/Atg14(L). Proc Natl Acad Sci U S A 108, 7769–7774 (2011). [PubMed: 21518905]
27. Baskaran S et al. Architecture and dynamics of the autophagic phosphatidylinositol 3-kinase complex. Elife 3, e05115 (2014).

28. Rostislavleva K et al. Structure and flexibility of the endosomal Vps34 complex reveals the basis of its function on membranes. Science 350, aac7365 (2015). [PubMed: 26450213]
29. Hope MJ, Bally MB, Webb G & Cullis PR Production of large unilamellar vesicles by a rapid extrusion procedure: characterization of size distribution, trapped volume and ability to maintain a membrane potential. Biochim Biophys Acta 812, 55–65 (1985). [PubMed: 23008845]
30. Mayer LD, Hope MJ & Cullis PR Vesicles of variable sizes produced by a rapid extrusion procedure. Biochim Biophys Acta 858, 161–168 (1986). [PubMed: 3707960]
31. Evans WH & Hardison WG Phospholipid, cholesterol, polypeptide and glycoprotein composition of hepatic endosome subfractions. Biochem J 232, 33–36 (1985). [PubMed: 2867761]
32. Kobayashi T et al. A lipid associated with the antiphospholipid syndrome regulates endosome structure and function. Nature 392, 193–197 (1998). [PubMed: 9515966]
33. Carlton J et al. Sorting nexin-1 mediates tubular endosome-to-TGN transport through coincidence sensing of high- curvature membranes and 3-phosphoinositides. Curr Biol 14, 1791–1800 (2004). [PubMed: 15498486]
34. Polson HE et al. Mammalian Atg18 (WIPI2) localizes to omegasome-anchored phagophores and positively regulates LC3 lipidation. Autophagy 6, 506–522 (2010). [PubMed: 20505359]
35. Jose J, Tang J, Taylor AB, Baker TS & Kuhn RJ Fluorescent protein-tagged Sindbis virus E2 glycoprotein allows single particle analysis of virus budding from live cells. Viruses 7, 6182–6199 (2015). [PubMed: 26633461]
36. Maschkowitz G, Gartner S, Hofmann-Winkler H, Fickenscher H & Winkler M Interaction of human cytomegalovirus tegument proteins ppUL35 and ppUL35A with sorting nexin 5 regulates glycoprotein B (gpUL55) localization. J Virol 92, e00013–18 (2018). [PubMed: 29444945]
37. Schuchman R et al. Comparative Characterization of the Sindbis virus proteome from mammalian and invertebrate hosts identifies nsP2 as a component of the virion and sorting nexin 5 as a significant host factor for alphavirus replication. J Virol 92, e00694–18 (2018). [PubMed: 29743363]

Additional References

38. van Weering JR et al. Molecular basis for SNX-BAR-mediated assembly of distinct endosomal sorting tubules. EMBO J 31, 4466–4480 (2012). [PubMed: 23085988]
39. Durkin ME, Qian X, Popescu NC & Lowy DR Isolation of mouse embryo fibroblasts. Bio Protoc 3, e908 (2013).
40. Dowdle WE et al. Selective VPS34 inhibitor blocks autophagy and uncovers a role for NCOA4 in ferritin degradation and iron homeostasis in vivo. Nat Cell Biol 16, 1069–1079 (2014). [PubMed: 25327288]
41. Thoreen CC et al. An ATP-competitive mammalian target of rapamycin inhibitor reveals rapamycin-resistant functions of mTORC1. J Biol Chem 284, 8023–8032 (2009). [PubMed: 19150980]
42. Gobeil PA & Leib DA Herpes simplex virus gamma34.5 interferes with autophagosome maturation and antigen presentation in dendritic cells. MBio 3, e00267–00212 (2012). [PubMed: 23073763]
43. Taylor RM, Hurlbut HS, Work TH, Kingston JR & Frothingham TE Sindbis virus: a newly recognized arthropodtransmitted virus. Am J Trop Med Hyg 4, 844–862 (1955). [PubMed: 13259009]
44. Hardwick JM & Levine B Sindbis virus vector system for functional analysis of apoptosis regulators. Methods Enzymol 322, 492–508 (2000). [PubMed: 10914042]
45. Schuffenecker I et al. Genome microevolution of chikungunya viruses causing the Indian Ocean outbreak. PLoS Med 3, e263 (2006). [PubMed: 16700631]
46. Keller BC et al. Resistance to alpha/beta interferon is a determinant of West Nile virus replication fitness and virulence. J Virol 80, 9424–9434 (2006). [PubMed: 16973548]
47. Melnick JL et al. Isolation from human sera in Egypt of a virus apparently identical to West Nile virus. Proc Soc Exp Biol Med 77, 661–665 (1951). [PubMed: 14891830]
48. Huang da W, Sherman BT & Lempicki RA Systematic and integrative analysis of large gene lists using DAVID bioinformatics resources. Nat Protoc 4, 44–57 (2009). [PubMed: 19131956]

49. Huang da W, Sherman BT & Lempicki RA Bioinformatics enrichment tools: paths toward the comprehensive functional analysis of large gene lists. Nucleic Acids Res 37, 1–13 (2009). [PubMed: 19033363]
50. Honess RW & Roizman B Regulation of herpesvirus macromolecular synthesis. I. Cascade regulation of the synthesis of three groups of viral proteins. J Virol 14, 8–19 (1974). [PubMed: 4365321]
51. Sawicki DL, Sawicki SG, Keranen S & Kaariainen L Specific Sindbis virus-coded function for minus-strand RNA synthesis. J Virol 39, 348–358 (1981). [PubMed: 7277580]
52. Axe EL et al. Autophagosome formation from membrane compartments enriched in phosphatidylinositol 3-phosphate and dynamically connected to the endoplasmic reticulum. J Cell Biol 182, 685–701 (2008). [PubMed: 18725538]
53. Steinberg F et al. A global analysis of SNX27-retromer assembly and cargo specificity reveals a function in glucose and metal ion transport. Nat Cell Biol 15, 461–471 (2013). [PubMed: 23563491]
54. Ma M et al. Cryo-EM structure and biochemical analysis reveal the basis of the functional difference between human PI3KC3-C1 and -C2. Cell Res 27, 989–1001 (2017). [PubMed: 28731030]

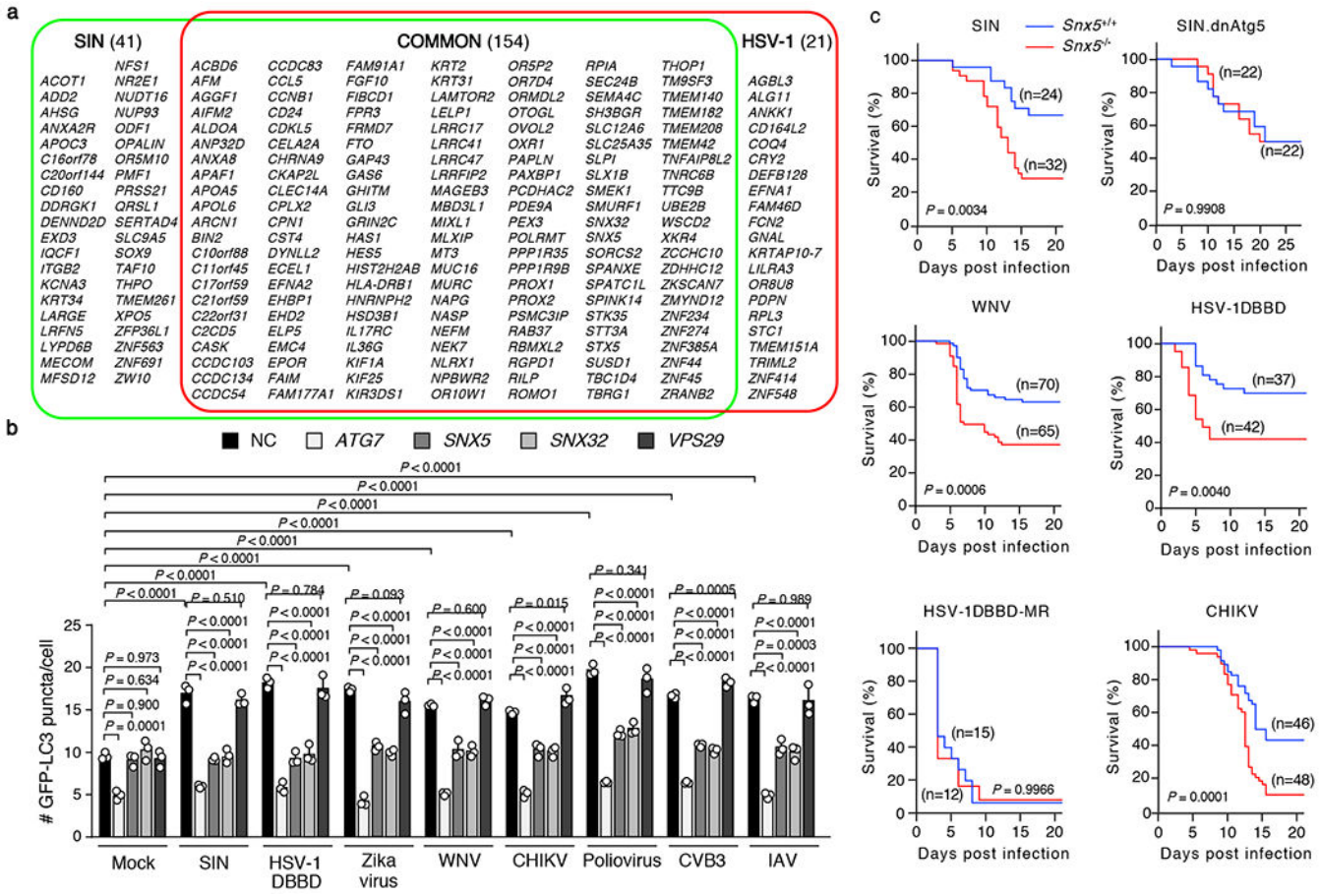

Fig. 1. SNX5 is required for virus-induced autophagy *in vitro* and antiviral host defense *in vivo*.

a, Confirmed hits from deconvolution siRNA screens grouped according to their requirement for SIN-induced autophagy, HSV-1ΔBBD-induced autophagy, or both. **b**, GFP-LC3 puncta in HeLa/GFP-LC3 cells treated with indicated siRNAs (72 h) and mock-infected or infected with indicated virus for 4.5 h. MOI = 5 for HSV-1ΔBBD; 10 for SIN, Zika virus, WNV, CHIKV and IAV; and 20 for poliovirus and CVB3. Bars represent mean ± s.d. of three independent replicates (100-150 cells per sample). *P*-values, one-way ANOVA with Dunnett's test for multiple comparisons. **c**, Survival of $Snx5^{+/+}$ and $Snx5^{-/-}$ mice infected with SIN (strain dsTE12Q, 1,000 pfu i.c., 7-day-old mice), SIN.dnAtg5 (1,000 pfu i.c., 7-day-old mice), HSV-1ΔBBD (50,000 pfu i.c., 8 to 10-week-old mice), HSV-1ΔBBD-MR (50,000 pfu i.c., 8 to 10-week-old mice), WNV (1 pfu i.c., 5.5-day-old mice) or CHIKV (100,000 pfu s.c., 7-day-old mice). Results represent combined data for at least three independent experiments per virus; similar results obtained for each infection. *P*-values, log-rank test (two-sided).

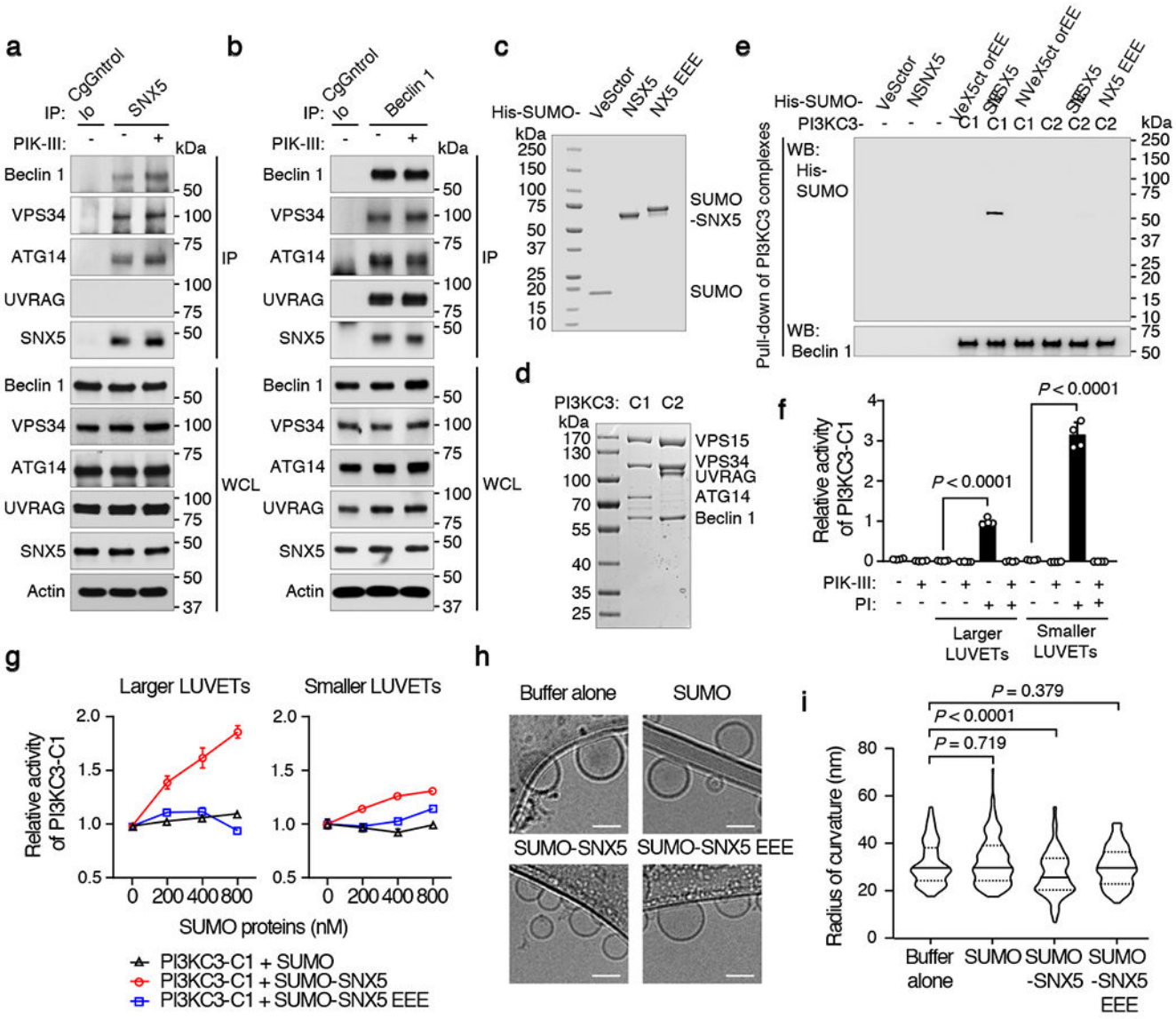

Fig. 2. SNX5 interacts with PI3KC3-C1 complex and augments its lipid kinase activity.

a, **b**, Western blots showing co-immunoprecipitation of endogenous PI3KC3 complex proteins with SNX5 (**a**) or beclin 1 (**b**) in HeLa cells treated with DMSO or PIK-III (5 μM, 1 h). IP, immunoprecipitates; WCL, whole cell lysates. **c**, **d**, Coomassie blue staining of His-tagged SUMO, SUMO-SNX5 or SUMO-SNX5 EEE (**c**) or PI3KC3 complexes purified from HEK293F cells co-transfected with plasmids expressing beclin 1, VPS34, VPS15 and either ATG14 (PI3KC3-C1) or UVRAG (PI3KC3-C2) (**d**). **e**, Western blot of His-tagged proteins in eluates from *in vitro* binding with PI3KC3 complexes. Similar results for **a-e** were observed in three independent experiments. **f**, Relative PI3KC3-C1 activity in an *in vitro* lipid kinase assay using either PI^- or PI^+ LUVETs +/− PIK-III (0.5 mM). Bars represent mean ± s.d., n=4 biologically independent samples. *P*-values, unpaired two-tailed *t*-tests. PI3KC3-C1 has higher activity on smaller PI^+ LUVETs (*P* = 2.1e-8; two-way ANOVA). **g**, Relative PI3KC3-C1 activity (normalized to 0 nM SUMO) in an *in vitro* lipid

kinase assay using PI^+ LUVETs with indicated SUMO-fusion protein. Symbols represent mean ± s.d., n=4 biologically independent samples. The dose-dependent SUMO-SNX5-mediated increase in lipid kinase activity is greater on larger LUVETs ($P = 0.000035$; linear regression with three-way interaction term). **h**, **i**, Representative cryo-EM micrographs (**h**) and violin plots of the radius of curvature for vertex points (**i**) of larger PI^+ LUVETs incubated for 30 min with buffer alone or indicated proteins (>150 liposomes per sample). Scale bar, 60 nm. *P*-values, one-way ANOVA with Dunnett's test for multiple comparisons. See Supplementary Fig. 1 for gel source data.

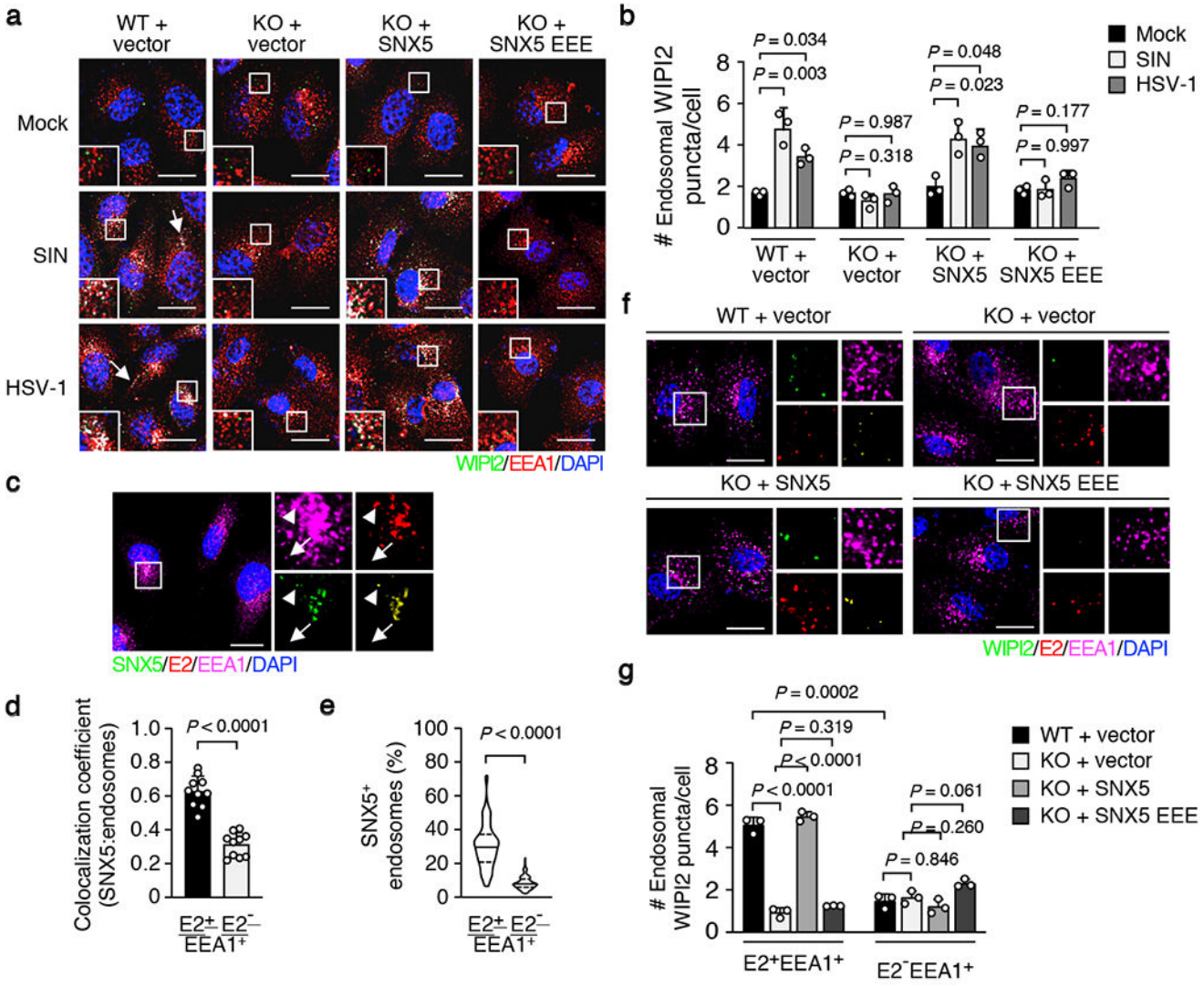

Fig. 3. SNX5 is required for virus-induced endosomal generation of PI3P.

a, **b**, Representative fluorescent micrographs (**a**) and quantitation (**b**) of WIPI2$^+$ (green) and EEA1$^+$ (red) puncta in indicated cells. Scale bars, 20 μm. Arrows denote representative WIPI2$^+$EEA1$^+$ puncta (white) that would score positive in **b**. Insets, 4X magnification of boxed areas. Error bars, mean ± s.d. (three replicates, 100-150 cells each). **c**-**e**, Representative fluorescent micrographs (**c**) and quantitation (**d**, **e**) of SNX5 endosomal localization in SIN.mCherry-E2-infected HeLa cells (MOI = 10, 1 h). Scale bars, 20 μm. Boxed areas are magnified 9X (right) to show SNX5 (green), E2 (red) and EEA1 (magenta) and SNX5$^+$E2$^+$EEA1$^+$ colocalization (yellow). Arrows and arrowheads denote representative SNX5$^-$E2$^-$EEA1$^+$ and SNX5$^+$E2$^+$EEA1$^+$ endosomes, respectively. Bars in **d** represent mean ± s.d. of Manders' overlap coefficient of SNX5 and E2$^+$EEA1$^+$ or E2$^-$EEA1$^+$ colocalization (n=10, >40 cells per replicate). **e,** Violin plots of percentage of overlapping SNX5$^+$ and E2$^+$EEA1$^+$ or E2$^-$EEA1$^+$ puncta (n=137 cells). **f**, **g**, Representative fluorescent micrographs (**f**) and quantitation (**g**) of endosomal WIPI2 puncta in indicated

cells. Scale bars, 20 μm. Boxed areas are magnified 4X (right) to show WIPI2 (green), E2 (red) and EEA1 (magenta) and $WIPI2^+E2^+EEA1^+$ colocalization (yellow). Yellow puncta represent $WIPI2^+E2^+EEA1^+$ puncta that would score positive in **g**. Bars in **g** represent mean ± s.d. (n=3, 100-150 cells per replicate). *P*-values, one-way ANOVA with Dunnett's test for multiple comparisons (**b**, **g**) or unpaired two-tailed *t*-test (**d**, **e**). Similar results obtained from three independent experiments.